X-602-75-281

PREPRINT

NASA TM X- 71060

THEORY OF TYPE IIIb SOLAR RADIO BURSTS

ROBERT A. SMITH
JÉRÔME de la NOË

OCTOBER 1975

GSFC — GODDARD SPACE FLIGHT CENTER —
GREENBELT, MARYLAND

THEORY OF TYPE IIIb SOLAR RADIO BURSTS

Robert A. Smith*†
Theoretical Studies Group
Goddard Space Flight Center
Greenbelt, Maryland 20771

and

Jérôme de la Noë†
Astronomy Program
University of Maryland
College Park, Maryland 20742

*NAS/NRC Postdoctoral Resident Research Associate
†Present address: Paris Observatory, 92190 Meudon, France

ABSTRACT

During the initial space-time evolution of an electron beam injected into the corona, the strong beam-plasma interaction occurs at the head of the beam, leading to the amplification of a quasi-monochromatic large-amplitude plasma wave that stabilizes by trapping the beam particles. Oscillation of the trapped particles in the wave troughs amplifies sideband electrostatic waves. The sidebands and the main wave subsequently decay to observable transverse electromagnetic waves through the parametric decay instability. This process gives rise to the elementary striation bursts. Owing to velocity dispersion in the beam and the density gradient of the corona, the entire process may repeat at a finite number of discrete plasma levels, producing chains of elementary bursts. All the properties of the type IIIb bursts are accounted for in the context of the theory.

I. INTRODUCTION

The so-called type III^b solar radio burst was defined by de la Noë and Boischot (1972) as a chain of several elementary bursts which appear in dynamic spectra as either single, double, or triple narrow-banded striations (Figure 1). The spectral features of these striations were described extensively by Ellis and McCulloch (1966, 1967) and de la Noë (1975). We shall describe here the salient characteristics of the bursts, which will be theoretically explained in this paper.

A. Properties of Elementary Bursts

1. Individual striations exhibit a very narrow bandwidth Δf: the average is approximately 100 kHz, but Δf may vary from the frequency resolution of the receivers ($\sim$ 15 kHz) to a few hundreds of kHz.

2. In double- or triple-striation groups, the frequency separation δf, between the edges of the individual striations, is also approximately 100 kHz on the average, with less-dispersed limits than for Δf.

3. The duration at a given frequency varied from the time resolution of the receivers ($\sim$ 20 ms) to a few s; the average duration is about 1 s, a factor of $\sim$ 4.5 lower than the duration of normal type III bursts (Aubier and Boischot 1972, de la Noë 1975).

4. These short, quasi-monochromatic bursts are observed at frequencies between 100 MHz and 10 MHz. No such bursts have ever been reported at higher frequencies. A search by one of the authors (J.L.N.) to detect them at lower frequencies among satellite observations by IMP-6 and RAE-2 was negative, possibly because of the frequency and time resolutions of these experiments. The occurrence of elementary bursts was found to peak around 30 MHz (de la Noë and Boischot 1972), at least

for the studied period July-August 1970.

5. Circular polarization is observed for the striations, but it occurs in a totally random way from one to another elementary burst in a chain. However, when doublet or triplet elementary bursts are found polarized, all the striations have the same sense of circular polarization.

6. In a few cases ($\sim$ 20 %), elementary bursts were found to have a non-zero drift rate towards lower frequencies. When it occurs, this frequency drift affects most striations occurring in a short period of time. The drift rate may reach values up to -150 kHz/s, but in most cases is null or not measurable.

B. Properties of Type III b Bursts

Besides the intrinsic properties of the elementary bursts, described above, the properties of chains of elementary bursts lead to interesting clues to understanding the phenomenon.

1. The leading edge of the spectral envelope of type IIIb bursts is similar to that of type III bursts. This suggests not only their appellation, but also that the type IIIb bursts are produced by the same kind of exciter as type III bursts: viz., electron streams with average velocity $\sim$ c/3 (Lin, Evans, and Fainberg 1973).

2. de la Noë and Boischot (1972) found that 30% of type IIIb bursts were precursors to type III bursts, strengthening the hypothesis of a common agent for both types of bursts. de la Noë (1974) showed that this relationship, which could be owing to pure association, was real mainly when the sources of the bursts are located near the limb,

although location of sources on the central part of the disk does not preclude such association. Type IIIb bursts seem to be emitted at a large angle to the local magnetic field, rather than along the field.

3. A recent study of type III bursts by Rosenberg (1974) led that author to conclude that 95% of all type III bursts occur at $\simeq 2\ \omega_e$, where ω_e is the local plasma frequency. When a type IIIb burst is seen as a precursor to a type III, the measured frequency ratio f_{III}/f_{IIIb} at a given time is somewhat dispersed. It suggests, however, that emission of the type IIIb burst takes place close to ω_e, while the type III is at $2\omega_e$. This assumption is strengthened by the recent observation of both fundamental and harmonic emissions of a type U burst, in which the fundamental is striated while the harmonic emission is smooth (Stewart 1975).

4. Positional measurements of precursor type IIIb and following type III bursts showed that both emissions are located at the same place in the corona (de la Noë and Gergely 1975). This strengthens the hypothesis that both bursts are excited by the same electron stream with two different mechanisms: the first produces the type IIIb burst, takes place at the front of the beam and requires a shorter time to generate the emission; the second one which generates the type III burst is a process like that studied by Papadopoulos, Goldstein, and Smith (1974).

C. Outline of the Theory

We assume that the particles are injected from a localized acceleration region in the lower corona, forming a beam which is guided by the magnetic field. The velocity dispersion in the beam causes a time-dependent evolution of the distribution function at any point in space. For some time after the beginning of the injection, no particles will have arrived at, say, the point x. Then the fastest particles in the beam

arrive at x, followed by successively slower particles. For some time during this evolution, the quantity V_b/U is very small, where V_b is the thermal spread that characterizes the velocity range over which the beam distribution rises to its instantaneous peak at the velocity U. In the theory that follows, we shall assume

$$\frac{V_b}{U} < \eta^{1/3}, \tag{1.1}$$

where $\eta \equiv n_b/n_e$ is the instantaneous ratio of the beam density to that of the ambient plasma. Although the condition (1.1) may seem stringent, it is quite easy to construct models of the beam evolution in which (1.1) is satisfied. To preserve the continuity of the present discussion, we defer to Appendix A a fuller examination of the evolution of the beam. Here and in what follows we shall simply assume that inequality (1.1) is satisfied at some time in the early evolution of the beam at a given point. In Appendix A we show that this assumption appears justified under a wide range of plausible conditions for the injection of the beam into the corona.

We may now discuss the salient features of the theory that follows. When a beam satisfying inequality (1.1) propagates through a background plasma, quasi-monochromatic plasma waves, with phase velocities just below the beam velocity U, are unstable with exponential growth rate $\gamma \simeq \eta^{1/3}\,\omega_e$. We refer to this regime as the strong beam-plasma interaction, in contrast to the so-called "bump-on-tail" instability in which inequality (1.1) is reversed and a broad band of waves grows at approximately the rate $\eta\omega_e$. In the strong-interaction regime, the growth of the beam-mode waves is saturated by trapping of the beam particles. The oscillation of the trapped particles in the wave troughs gives rise to unstable sideband waves, separated in frequency from the main wave by approximately the bounce frequency of the particles. The main wave and the sidebands, which are all electrostatic

oscillations, subsequently decay into transverse waves, at approximately the plasma frequency, and ion-acoustic waves. In addition, as the sidebands grow to amplitudes comparable to that of the main wave, the particles experience a demodulation of the wave phases; i.e., the autocorrelation time becomes of the order of the bounce period. The particles are then no longer trapped. After a certain distance, however, owing to the velocity dispersion of the beam and the density gradient of the corona, the beam will again satisfy condition (1.1) and the entire process may repeat.

We now discuss each facet of the theory in turn.

II. THE BEAM-PLASMA INTERACTION

The interaction of a cold low-density beam with a plasma has been investigated by O'Neil and Malmberg (1968), Drummond et al. (1970), and O'Neil, Winfrey, and Malmberg (1971). We shall consider an electron beam injected into a neutral background plasma. This system is not charge-neutral, and a return current flows with velocity ηU. As was shown by Melrose (1974), the effects of the return current are negligible for conditions appropriate to type III bursts, and so we consider the ions to be a fixed neutralizing background. As usual, we consider a one-dimensional interaction. Then the dispersion relation for electrostatic waves is

$$1 - \frac{\omega_e^2}{k^2} \int_{-\infty}^{\infty} dv \; \frac{k \, \partial F_e/\partial v}{kv-\omega} - \eta \, \frac{\omega_e^2}{k^2} \int_{-\infty}^{\infty} dv \; \frac{k \, \partial F_b/\partial v}{kv-\omega} = 0, \qquad (2.1)$$

where ω_e is the electron plasma frequency, and F_e, F_b are the distribution functions of the ambient and beam electrons, respectively.

Following O'Neil and Malmberg (1968), we take the beam distribution to be Lorentzian:

$$F_b(v) = \frac{V_b}{\pi} \frac{1}{(v-U)^2 + V_b^2}, \qquad (2.2)$$

where V_b measures the velocity spread. The assumption of the form (2.2) for F_b is a matter of convenience; O'Neil and Malmberg showed that results similar to those below are obtained by taking F_b to be Maxwellian. The principal advantage of the form (2.2) is that it enables one to evaluate the resonance

integral for the beam in Eq. (2.1) easily*;

$$\frac{1}{k^2}\int_{-\infty}^{\infty} dv \ \frac{k\ \partial F_b/\partial v}{kv-\omega} = (\omega - kU + ik\ V_b)^{-2}. \tag{2.3}$$

We denote the plasma dielectric

$$\varepsilon_o(k,\omega) = 1 - \frac{\omega_e^2}{k^2}\int_{-\infty}^{\infty} dv \ \frac{k\ \partial F_e/\partial v}{kv-\omega}.$$

Then, assuming

$$\exp\ (-U^2/2V_e^2) << \eta, \tag{2.4}$$

where $V_e = (T_e/m)^{\frac{1}{2}}$ is the electron thermal velocity, $\varepsilon_o(k,\omega)$ has an approximate zero at the point

$$\begin{aligned} \omega_o &= \omega_e\ (1 + 3\ \frac{k_o^2 V_e^2}{\omega_e^2})^{\frac{1}{2}}, \\ k_o &= \omega_o/U. \end{aligned} \tag{2.5}$$

Inequality (2.4) is easily satisfied under conditions of interest to us, in which we assume $5 \lesssim U/V_e \lesssim 20$ and $10^{-8} \lesssim \eta \lesssim 10^{-6}$. Then, using (2.3), the dispersion relation (2.1) may be expanded about (ω_o, k_o) to give (O'Neil et al. 1971)

$$\left[\left(\frac{\partial \varepsilon_o}{\partial \omega}\right)_{\omega_o,k_o}\omega' + \left(\frac{\partial \varepsilon_o}{\partial k}\right)_{\omega_o,k_o}k'\right](\omega' - k'U)^2 = \eta\ \omega_e^2, \tag{2.6}$$

where $\omega' \equiv \omega - \omega_o$ and $k' \equiv k - k_o$. In the present context, the waves

*We note that Eq. (2.2) implies an infinite energy density for the beam. This will be of no concern to us, since we shall not take moments of the distribution (2.2) but instead merely take advantage of its analytic properties. Note that (2.2) is a representation of the Dirac delta-function in the limit $V_b \to 0$.

vary as exp $i(kx - \omega t)$, so that Im $\omega' > 0$ implies instability. The integral in $\varepsilon_o(k,\omega)$ is to be performed on the usual Landau contour. Then we have

$$\text{Re}\ \varepsilon_o(k,\omega) = 1 - \frac{\omega_e^2}{\omega^2} - \frac{3\,\omega_e^4}{\omega^4}\, k^2 \lambda_{De}^2 - \cdots ,$$

where λ_{De} is the electron Debye length, and so

$$\begin{aligned} \omega_o \left(\frac{\partial \varepsilon_o}{\partial \omega}\right)_{(\omega_o,k_o)} &= -2(1 + 3\xi^2), \\ k_o \left(\frac{\partial \varepsilon_o}{\partial k}\right)_{(\omega_o,k_o)} &\simeq 6\xi^2(1 - 7\xi^2), \end{aligned} \tag{2.7}$$

where $\xi \equiv V_e/U$. Differentiating (2.6) with respect to k', using (2.7), and maximizing $\gamma_b \equiv \text{Im}\ \omega'$, one finds that maximum growth occurs at $k' = 0$, where the real frequency ω and growth rate γ_b are given by

$$\begin{aligned} \omega &= \omega_o(1 - \tilde{\eta}^{1/3}/2^{4/3}), \\ \gamma_b &= (3^{1/2}/2^{4/3})\, \tilde{\eta}^{1/3}\, \omega_o, \end{aligned} \tag{2.8}$$

where $\tilde{\eta} \equiv \eta\ (\omega_e^2/\omega_o^2) \left[(\omega_o/2)\ (\partial\varepsilon_o/\partial\omega)_{\omega_o,k_o}\right]^{-1}$. Note that ω_o, given by Eq. (2.5), contains the Bohm-Gross dispersion for a warm plasma. In this limit ($V_b/U < \eta^{1/3}$), the instability is reactive. The group velocity V_g is given by

$$V_g = \frac{d\omega}{dk} = \frac{2}{3} U + \frac{1}{3} \frac{V_e^2}{U} . \tag{2.9}$$

Furthermore, the half-width in k-space of $\gamma_b(k)$ is given approximately by

$$\Delta k \simeq \frac{1}{\gamma_b}\left|\frac{\partial^2\gamma_b}{\partial k^2}\right|^{-\frac{1}{2}}_{\gamma=\gamma\ \max} = \frac{3}{2^{5/6}}\,\eta^{1/3}\,k_o. \qquad (2.10)$$

We consider that the unstable waves grow out of the small thermal noise level present before the beam enters the plasma. Then many growth times γ^{-1} will pass before nonlinear effects become important. After N e-foldings ($t = N\,\gamma_b^{-1}$), the half-width of the unstable wave spectrum will be

$$\delta k = (\ln 2/N)^{\frac{1}{2}}\,\Delta k;$$

i.e.,

$$|E(k_o \pm \delta k)|^2 = \frac{1}{2}\ |E(k_o)|^2.$$

The waves stabilize by trapping particles when their amplitudes become sufficiently large to alter significantly the reactive orbits of the particles (O'Neil 1965, O'Neil et al. 1971). This process occurs only over the last few e-foldings. The question then becomes whether the spectral width δk is sufficient to destroy the autocorrelation of the spectrum in a time γ_b^{-1}. The phase difference seen by an electron of velocity v in this time interval is given by

$$\Delta\phi = |\,v - v_g\,|\,\gamma_b^{-1}\,\delta k,$$

and for autocorrelation to be maintained we require $\Delta\phi \ll 1$. For the plasma electrons this condition becomes

$$N^{\frac{1}{2}} \gg \left[8(\ln 2)/3\right]^{\frac{1}{2}}, \qquad (2.11)$$

and for the beam electrons

$$N^{\frac{1}{2}} >> \left[2(\ln 2)/3\right]^{\frac{1}{2}}. \tag{2.12}$$

Subsequent to trapping, the beam particles exchange energy with the wave; the exchange of energy occurs with the bounce frequency

$$\omega_B = (ek_0 E_s/m)^{\frac{1}{2}}, \tag{2.13}$$

where E_s is the saturation amplitude of the wave. Violation of inequality (2.11) causes nonresonant velocity diffusion of the background electrons, while violation of (2.12) causes resonant velocity diffusion of the beam electrons. For our purposes only the latter is of direct concern. We shall see below that under conditions of interest to us, the sides of (2.12) are in the ratio of order 5:1. Thus, it might appear that $N^{-\frac{1}{2}}$ is only marginally valid as a small parameter. Nevertheless, several recent experiments and theoretical studies indicate that the single-wave theory is valid despite the implications of inequality (2.12). In order not to interrupt our exposition here, we present a discussion of this point in Appendix B. In what follows, we assume that the single-wave theory is valid for times of the order of several bounce periods after saturation of the main wave.

At saturation, the time-averaged energy density of the trapping wave (averaged over one period) is given by

$$\frac{E_s^2}{16\pi} \simeq 2^{-4/3}\, \eta^{1/3}\, (n_b\, m\, U^2/2) = 2^{-4/3}\, \eta^{4/3}\, \frac{U^2}{V_e^2}\, n_e\, T_e, \tag{2.14}$$

where T_e is the temperature (in eV) of the background plasma.

III. THE SIDEBAND INSTABILITY

The motion of the particles trapped in the large-amplitude-wave troughs is significantly distorted from the trajectories given by linear analysis. In the instantaneous frame moving with the phase velocity of the trapping wave, the trapped particles execute closed orbits in phase space (Fig. 2), whereas untrapped particles move unidirectionally over the wave with a sinusoidal modulation of their velocities relative to the wave. The amplitude of this modulation is

$$v_{os} \simeq e E_s/m \omega. \tag{3.1}$$

The distortion of the orbits of the trapped particles leads to the coupling of the main wave to sideband waves at frequencies $\omega_0 \pm \omega_B$, where the bounce frequency ω_B is given by Eq. (2.13). The parametric sideband instability has been examined by Kruer, Dawson, and Sudan (1969), Goldman and Bark (1971), and Wong (1972). Other recent treatments have been given by Bud'ko, Karpman, and Shklyar (1971), and by Brinca (1972). In this section we shall present only the salient points to be used in the remainder of this work; additional remarks about the sideband instability are given in Appendix B.

The initial observation of such sidebands was reported by Wharton, Malmberg, and O'Neil (1968). In the experiment by Wharton et al., a large-amplitude wave was launched into a plasma. In such a situation, the trapped electrons separate generally into two classes: "resonant" particles which are trapped near the bottom of the wave trough, and "nonresonant" particles which oscillate on trajectories near the separatrix of Figure 2. Generally speaking, the resonant particles execute closed trajectories in

phase space with the bounce frequency ω_B, while the nonresonant particles take an arbitrarily long time to execute a closed orbit. The treatments of Kruer et al. (1969) and Wong (1972) are appropriate to this situation.

In our case, however, we are dealing not with a large-amplitude wave launched into the plasma, but rather with a wave which grows from thermal noise on a beam. In this situation, nearly all the particles are resonant. The theoretical treatment appropriate to this case is that of Goldman and Berk (1971).

Let us denote the frequency and wavenumber of the trapping wave by $\bar{\omega}_0$ and $\bar{k}_0$, respectively. Then the principal sideband waves are at frequencies $\omega = \bar{\omega}_0 + \Delta\omega$ and wavenumbers $k = \bar{k}_0 + \Delta k$ which are given by the dispersion relation of Goldman and Berk (1971)*:

$$\left[\Delta\omega - 3\,\frac{V_e^2}{U}\,\Delta k\right]^2 \left[(\Delta\omega - U\,\Delta k)^2 - \omega_B^2\right] - \varepsilon^2\,\omega_B^2\,(\Delta\omega - U\,\Delta k)^2 = 0, \tag{3.2}$$

where $\varepsilon \equiv \eta\,\omega_e^3/\omega_B^3$ under the assumption that all of the beam particles are trapped. From Eqs. (2.13) and (2.14), we find

$$\varepsilon = \eta\,(\eta\,E_s^2/4\pi\,n_b\,m\,U^2)^{-3/4} = 2.$$

*Here, Δk should not be confused with the Δk of Eq. (2.10).

In Figure 3(a) we have plotted the maximum sideband growth rate, and the wavenumber shift and frequency shift at which the maximum growth rate occurs, as a function of $\xi = V_e/U$; all quantities are normalized to ω_B. We see that all of these quantities are only weakly dependent on ξ in the range $0.1 \lesssim \xi \lesssim 0.2$, while they approach asymptotic values for $\xi \lesssim 0.1$. (For a coronal temperature of 2×10^6 K, a value of $\xi = 0.1$ corresponds to a beam energy $m\,U^2/2 \simeq 20$ kev, while $\xi = 0.2$ implies an energy $\simeq 5$ kev.) Furthermore, the results are found to be only weakly dependent on ε, in agreement with the results of Goldman and Berk. In addition, denoting $\Delta\omega = \Delta\omega_r + i\,\gamma_{sb}$, the solutions obey the symmetries

$$\begin{aligned} \Delta\omega_r\,(-\Delta k) &= -\,\Delta\omega_r\,(\Delta k), \\ \gamma_{sb}\,(-\Delta k) &= \gamma_{sb}\,(\Delta k). \end{aligned} \tag{3.3}$$

The growth rate $\gamma_{sb}\,(\Delta k)$ drops off sharply for $|\Delta k| > |\Delta k(\gamma_{max})|$ and tapers off more slowly for $|\Delta k| < |\Delta k(\gamma_{max})|$; the width in frequency $\Delta\omega_r$ between half-maxima is approximately ω_B. Analogously to the discussion of § II regarding the narrowing of the spectrum as the waves grow, the frequency width of the sidebands becomes $\lesssim .2\ \omega_B$ as the most unstable wave becomes comparable in amplitude to the main wave.

In Figure 3(b) we have replotted the results of Figure 3(a) normalized to ω_e for various values of η; from Eq. (2-14), the normalization is given by $\omega_B \simeq 2^{-1/12}\,\eta^{1/3}\,\omega_e$.

IV. THE PARAMETRIC DECAY INSTABILITY

Large-amplitude, quasi-monochromatic plasma waves are unstable to fixed-phase wave-coupling interactions known as parametric instabilities. In general, such instabilities may occur when there exists an approximate frequency-matching relation between the large-amplitude "pump" wave and two or more normal modes of the plasma. In contrast to weak-turbulence, random-phase interactions, however, the unstable modes may have dispersion properties different from those of the normal-mode waves; i.e., they may be eigenmodes only of the nonlinear plasma dielectric in the presence of the pump wave. A case in point is the oscillating-two-stream instability (Nishikawa 1968a,b; Sanmartin 1970), in which the pump is a dipole ($k=0$) plasma wave at the plasma frequency, the normal modes are a plasma wave with frequency higher than the pump wave ($k>0$) and an ion acoustic wave, and the unstable modes are frequency-shifted ion-acoustic and plasma waves with $|k|>0$. This instability was applied to the problem of the stabilization of the type III exciter by Papadopoulos et al. (1974).

Parametric instabilities are also characterized by the existence of a threshold amplitude which must be exceeded by the pump wave in order that instability may occur. In the present context, the only instability for which the threshold is exceeded is the decay of the Langmuir pump wave into a transverse electromagnetic (TE) wave and an ion-acoustic oscillation. This process was investigated by Lashmore-Davies (1974a,b).

Consider a Langmuir pump wave, a TE wave, and an ion-acoustic wave with frequencies ω_L, ω_T, and ω_S, respectively, and wave vectors $\vec{k}_L$, $\vec{k}_T$, and $\vec{k}_S$, respectively, such that

$$\vec{k}_L \simeq \vec{k}_T + \vec{k}_S \ ,$$
$$\omega_L \simeq \omega_T + \omega_S \ . \tag{4.1}$$

Denoting $\delta \equiv \omega_T - \omega_L$, we look for unstable modes with complex eigenfrequencies ω. Further denoting $\Omega \equiv \omega + \delta$, the dispersion relation for a traveling Langmuir-wave pump was shown by Lashmore-Davies (1974a,b) to be given by

$$(\Omega - \delta + i\,\gamma_T)\ (\Omega^2 - \omega_S^2 + 2\,i\,\gamma_S\Omega) - \tfrac{1}{2} K\,\omega_S = 0, \tag{4.2}$$

where γ_T, γ_S are the damping rates for the TE and ion-acoustic (S) waves, respectively, and where

$$K = \frac{1}{4}\ \frac{E_L^2}{8\pi\, n_e T_e}\ \omega_e^2 . \tag{4.3}$$

The dispersion relation (4.2) also describes the up-conversion of a plasma wave to a TE wave with higher frequency. In this case the matching relations are $\vec{k}_T = \vec{k}_L + \vec{k}_S$, $\omega_T \simeq \omega_L + \omega_S$, and $\delta > 0$. For $\gamma_T << \gamma_S$, the thresholds for the two processes are (Lashmore-Davies 1974a)

$$K_c = 4\,\gamma_S\,\gamma_T\,|\delta|/\omega_S \qquad , \delta<0 \ ;$$
$$K_c = 2\,\delta\,\omega_S \qquad , \delta>0. \tag{4.4}$$

In Eq. (4.4), the condition $|\delta| > (2\,\gamma_T/\gamma_S)^{\frac{1}{2}}\,\omega_S$ must also be satisfied. For $\gamma_T \simeq \omega_S$, the instability threshold for both $\delta \gtrless 0$ is $K_c = 4\,\gamma_S\gamma_T$, independent of δ. Therefore, we must estimate the relative magnitude of γ_T/ω_S and the value of K in both the main wave and sidebands.

To estimate K we assume that the sidebands grow to approximately the amplitude of the main wave. This assumption is suggested by the

observation that when multiple-striation elementary bursts appear, all elements in the burst group appear to be of roughly equal intensity. Furthermore, owing to the presence of the sideband waves, the particles experience wave phases of several times 2π during one bounce period; i.e., $\delta\omega = |\omega_{sb} - \omega_0| > \omega_B$. Therefore the particle motion becomes stochastic, rather than coherently modulated as in the trapping wave. Without examining the exact particle dynamics, it is reasonable to assume that this demodulation becomes important when all the waves are of approximately equal amplitude. Therefore, we estimate K for the sidebands as well as the main waves by substituting Eq. (2.14) into Eq. (4.3). The resulting value is

$$K_{sat} = \frac{\omega_e^2 \, \eta^{4/3}}{2^{7/3} \, \xi^2} , \tag{4.5}$$

where the subscript "sat" indicates that the saturation amplitude of the main wave has been used.

The value of γ_T to be used in determining whether or not K_{sat} exceeds K_c is the enhanced damping decrement determined by the presence of the ion-acoustic turbulence that is produced by the decay instability itself. If, however, the TE wave has a frequency which lies within the frequency range $\delta\omega$ of the driver wave packet -- either in the main wave or the sidebands -- then γ_T should be replaced by $\delta\omega$, which is an effective collision frequency. In Appendix C we estimate γ_T and show that with such considerations, the threshold values (4.4) are exceeded by K_{sat} only for $\delta<0$. In Figure 4.4 we plot K_{sat} and $K_{sat}/K_{c,sat}$ vs. ξ for $10^{-8} < \eta < 10^{-6}$. We see that the decay threshold is typically exceeded by factors of order 10-1000. It may therefore appear at first glance that K_{sat} is not the correct pump intensity

to use, because the decay instability will occur at smaller levels as the pump is growing. We shall see below, however, that even at the saturated amplitudes the decay rate γ_d is much smaller than γ_b and γ_{sb}. Thus the first three phases of the elementary burst process -- growth and saturation of the main wave, growth of the sidebands, and decay of all the waves -- occur on well-separated time scales.

We denote the wavenumber of the TE wave by k_T, and define $\alpha_T = ck_T/\omega_e$. Because $\alpha_T << 1$, the index of refraction

$$\frac{ck}{\omega} \simeq \alpha_T(1 - \alpha_T^2/2) \simeq \alpha_T.$$

Now consider the decay of a pump wave of phase velocity V_ϕ, and let $V \equiv V_e/V_\phi$. Then the frequency mismatch δ is given by

$$\frac{\delta}{\omega_e} = (1 + \alpha_T^2)^{\frac{1}{2}} - (1 + 3\,V^2)^{\frac{1}{2}}, \tag{4.6}$$

and

$$\frac{\omega_s}{\omega_e} = \mu^{\frac{1}{2}}(V - \alpha_T\, V_e/C) \simeq \mu^{\frac{1}{2}}\, V. \tag{4.7}$$

From (4.6), the range of δ is

$$0 \leq \frac{|\delta|}{\omega_e} \leq (1 + 3V^2)^{\frac{1}{2}} - 1.$$

As expected from the frequency matching condition $\omega_L \simeq \omega_T + \omega_S$, the growth rate of the decay instability is a maximum for $|\delta| = \omega_S$.

In Figure 5 we show (dashed curves) the maximum growth rate, calculated from the dispersion relation (4.2), as a function of V for various values of η. This rate is typically in the range $10^{-5} \lesssim \gamma_d/\omega_e \lesssim 10^{-3}$, and the functional form of the dashed curves in Figure 5 is

$$\frac{\gamma_d}{\omega_e} = 1.1 \times 10^{-2} \, \xi \, \frac{K_{sat}^{\frac{1}{2}}}{\omega_s} . \tag{4.8}$$

The dispersion relation (4.2), however, assumes a monochromatic pump spectrum, an approximation valid only as long as the growth rate γ_d is greater than the frequency width $\delta\omega$ of the pump. We have seen above that $\delta\omega \simeq 0.2 \, \omega_B$, and in general the condition of a monochromatic pump for the decay instability is invalid. In this case, we must modify the growth rate by the prescription (Valeo and Oberman 1973)

$$\gamma_d \to \gamma_d^2/\delta\omega,$$

and so we find

$$\frac{\gamma_d}{\omega_e} \simeq 5 \times 10^{-4} \, \frac{\xi^2 \, K_{sat}}{\eta^{1/3} \, \omega_s^2} . \tag{4.9}$$

The corrected value of γ_d given by (4.9) is shown in the solid curves of Figure 5. From Eqs. (4.6) and (4.7) we see that the index of refraction α_T of the TE wave for which γ_d is maximum (Figure 6) is independent of η and tends sharply to zero for $V \lesssim 0.05$. Therefore, we shall see below that only the range $V \gtrsim 0.05$ is of interest to us. The width of the decay spectrum, however, varies with η, and therefore a finite bandwidth in α_T is produced. In accord with our earlier convention, we define the width of the decay spectrum as that part of the spectrum for which $\gamma_d \geq .5 \, \gamma_{d,\,max}$. Then the bandwidth of the resulting TE spectrum is

$$\frac{\Delta\omega}{\omega} = \frac{\Delta\alpha_T}{\alpha_T}$$

In Figure 7 we plot this quantity. In the next section, we discuss these results in the context of the type IIIb observations.

V. APPLICATION TO TYPE IIIb BURSTS

As Noted in §I, the characteristics of elementary bursts vary widely about certain averages. We may understand this variability by noting that the growth rates and spectra of the various instabilities involved in the theory are somewhat sensitive to the instantaneous density and velocity of the beam (or, equivalently, the phase velocity of the decaying sidebands). These features are in turn determined by the overall intensity and shape of the beam velocity profile that is injected into the corona (see Appendix A), and these parameters may in principle vary widely among events. The corona itself is also variable in time, with regard to such features as its temperature and density profiles. Therefore, we can realistically ask of a theory for the type IIIb bursts only that it offer a framework within which the average phenomenological features of the bursts, and their range of variability, may be accounted for. In this section we show that the present theory meets this test. We shall focus first on the properties of the elementary bursts, and then consider how chains of such bursts may occur.

A. Properties of Elementary Bursts

1. Frequency Separation of the Striations

When two or three striations occur in an elementary burst, the frequency separation between them should be approximately the bounce frequency ω_B, according to the theory of the sideband instability (§III). At 30 MHz (the frequency of peak occurrence for type IIIb bursts), the average frequency separation δf is around 100 kHz. Thus $\delta f/f \simeq 3 \times 10^{-3}$;

equating

$$\frac{\delta f}{f} \simeq \frac{\omega_B}{\omega_e} \simeq \eta^{1/3}$$

gives an average value of 3×10^{-8} for η. Allowing for a factor of about 3 on either side of the average δf (which is not widely dispersed) leads us to consider the density range $10^{-9} < \eta < 10^{-6}$; the limits are extremes and the observations indicate the narrow range $10^{-8} \lesssim \eta \lesssim 10^{-7}$ as most typical. Thus we have presented numerical results for $\eta = 10^{-8}$ and 10^{-7}. That this is a reasonable range of η can be inferred from considerations of both the fundamental condition of the theory, given by inequality (1-1), and the contrasting requirements necessary for the development of the normal type III burst. Turning first to the latter of these considerations, we note that if (1-1) is violated, the growth rate of the weak beam-plasma instability is $\simeq \eta \omega_e$. The collisional damping rate is $\nu_e \simeq \omega_e/N_D$, where $N_D = n_e \lambda_{De}^3$ is typically of order (1-3) $\times 10^8$ in the lower corona. Therefore, a beam of instantaneous density $10^{-8} \lesssim \eta \lesssim 10^{-7}$, and in which condition (1-1) is violated, will be too weak to drive the linear beam-plasma instability. Conversely, (1-1) is most likely to be satisfied precisely at those times in the evolution when only the fastest particles have reached any particular point, and these particles constitute only a small fraction of the injected distribution.

2. Bandwidth and Frequency Range of Striations

As can be seen from Eq. (4.7), the refractive index of the TE wave is a function of the phase velocity V_ϕ of the decaying pump wave. In §I we noted that the typical bandwidth Δf of a striation was of order 100

kHz, ranging from <15 kHz to a few hundreds of kHz. At 30 MHz, this is a range of

$$5 \times 10^{-4} \lesssim \Delta f/f \lesssim 10^{-2},$$

with an average $\Delta f/f$ of about 3×10^{-3}. From Figure 7, we see that this implies

$$0.06 \lesssim V \lesssim 0.20 , \qquad (5.1)$$

where $V \equiv V_e/V_\phi$. For a coronal temperature of 2×10^6K, this corresponds to an energy range of $5 \lesssim E_e \lesssim 80$ kev, if the phase velocity V_ϕ is assumed to be equal to the beam velocity U. It is doubtful that electrons with energies as low as 5 kev actually play a role in type IIIb bursts, because under most conditions (1.1) is probably violated by the time the beam evolves down to such low energies. Figure 7 indicates, however, that whether or not V_ϕ is equated to U, we need to consider V_ϕ in the range (5.1).

The role of V is fundamentally to determine the frequency of the pump via the Bohm-Gross dispersion relation. Therefore the sidebands, which are shifted from the trapping wave by about twice the bounce frequency, are described for purposes of the decay instability by effective phase velocities different from that of the central trapping wave. Denoting by V_o, V_+ and V_- the ratios of V_e to the phase velocities of the main wave, upper and lower sidebands, respectively, we have

$$V_\pm = \frac{1}{\sqrt{3}} \left\{ \left[(1 + 3 V_o^2)^{\frac{1}{2}} \pm \frac{\Delta\omega_r}{\omega_e} \right]^2 - 1 \right\}^{\frac{1}{2}} \qquad (5.2)$$

where $\Delta\omega_r$ is given as a function of V_0 and η by Figure 3a. In Figure 8 we show $V_\pm$ corresponding to V_0 for various η. Note particularly that at low values of V_0, V_- may be $\lesssim 0.05$. As noted above, at $V \lesssim 0.05$ the refractive index of the daughter TE waves decreases rapidly (Figure 6). This is of

great significance when we consider the question of why elementary bursts most commonly consist of one striation, less frequently of a pair of striations, and only very occasionally of a triplet group.

3. Single- vs. Multiple-Striation Bursts

To understand this, let us consider the attenuation of the transverse waves by collisional absorption in the corona. For frequencies near the plasma frequency, the absorption per unit length is given by

$$\kappa \simeq \frac{\nu_c}{V_g} = \frac{\nu_c}{c^2}\frac{\omega_e}{k_T} = \frac{\nu_c}{c\alpha_T} \quad . \tag{5.3}$$

Because the wave is propagating through a medium of decreasing density, the optical depth τ may be approximated by

$$\tau \simeq \kappa L, \tag{5.4}$$

where $L \equiv n_e \left| dn_e/dr \right|^{-1}$ is the scale length of the coronal density gradient, Thus

$$\tau \simeq \tau_o/\alpha_T,$$

where $\tau_o \equiv \nu_c L/c$. In Figure 9 we show values of L and τ_o derived from three coronal density models which represent a wide range of coronal conditions, ranging from the quiet corona at solar maximum (Leblanc, Leroy, and Pecantet 1973) to Newkirk's active streamer model (Newkirk 1967), to an intermediate state (Riddle 1974). We see that τ_o ranges from values of $\lesssim 0.1$ at 30 MHz to $\gtrsim 0.4$ at 100 MHz. On the other hand, we see from Figure 6 that pump waves in the range $0.05 \lesssim V \lesssim 0.15$ decay to TEm waves with $0.07 \lesssim \alpha_T \lesssim 0.20$. Therefore, at any frequency, the higher the frequency of the decay pump, the higher the index of refraction of the daughter TE wave and the lower the attenuation factor $\exp(-\tau_o/\alpha_T)$. As a specific illustration, we combine in Figure 10 information from Figures 6, 8, 9 to

show the optical depth of the three possible elements in a triplet, at 30 MHz and 100 MHz, using Riddle's density model and an assumed density ratio $\eta = 10^{-7}$. The main wave phase velocity V_ϕ can be equated to U, so that $V_o = \xi$. We note that at 100 MHz the waves suffer severe attenuation at all V_o. At 30 MHz τ becomes <1 for the lower sideband only at $V_o = 0.09$, corresponding to beam energies of ≃25 kev.

At all frequencies and at all beam velocities, $\tau^+ < \tau^o < \tau^-$ (where the superscripts o, +, - refer to the main wave and the upper and lower sidebands, respectively). Depending on the frequency, however, one or more of the waves may suffer severe attenuation by $\exp(-\tau)$ between the source and the observer. For example, note that although both the main-wave and the upper-sideband daughters suffer little attenuation at 30 MHz, a similar calculation at 60 MHz would lead to $\tau^o < 1$ only for $V_o = \xi > 0.10$, while the corresponding value of τ^+ is 0.8.

The optical depth, especially defined only approximately as in Eq. (5.4), is admittedly a rough measure, and these arguments are meant to be suggestive rather than definitive. Nevertheless, because under most conditions we would expect condition (1-1) to be satisfied principally in a narrow range of ξ, probably bounded above by $\xi < 0.10$, the consideration of the attenuation of the various members in the elementary bursts offers a very plausible explanation of why single striations -- corresponding to the upper sideband only -- are seen about 80% of the time, while doublets -- decay products of the upper sideband plus main wave -- are seen about 20% of the time, and triplets, which require unusual conditions to be met by the beam, are rarely seen. It also explains why type IIIb bursts are not observed at frequencies greater than about 100 MHz; at such frequencies, τ_o is

relatively large, and severe attenuation of the emission would be expected to occur. (An explanation is given below for why bursts are not observed at lower frequencies.)

We have stressed the variability in the bursts owing to the variability of the beam evolution, because of the fundamental importance of condition (1-1) and because the dependence of the instability parameters on $\xi = V_e/U$ is easily seen. We note, however, that variations in the corona, such as temperature variations, for example, may also be important in determining the local parameter regime. An indication that this may be the case is the fact that despite the arguments above, which suggest that multiple-striation bursts ought to occur more commonly with decreasing frequency, we have not found a strong correlation between frequency and the number of elements in a burst group. This could be due, for example, to the decrease in temperature with decreasing plasma frequency, which would tend to keep $\xi = V_e/U$ at low values and suppress the lower sideband.

4. Duration of the Elementary Bursts

Let us turn to the topic of the observed duration of the burst at a given frequency. We assume for the moment that this duration is equal to the duration of the decay-instability phase, which we denote by $\bar{t}$. In § I we noted that the observed duration varies from less than 20 ms to a few seconds, but that its average value is about 1 s. As noted in § IV, we may write the maximum growth rate of the decay instability as

$$\gamma_d = 5 \times 10^{-4} \xi^2 \tilde{K} \eta^{-1/3} \omega_e, \tag{5.5}$$

where $\tilde{K} \equiv K/\omega_s^2$. Then the equation for the normalized TE energy density $\tilde{T}$ is

$$\frac{d\tilde{T}}{dt} = \gamma_d (\tilde{K}) \tilde{T}, \tag{5.6}$$

while

$$\frac{d\tilde{K}}{dt} = - \frac{d\tilde{T}}{dt} \quad , \tag{5.7}$$

where in (5.7) we have neglected the energy of the ion-acoustic waves compared to that of TE waves. Analogously to $\tilde{K}$, $\tilde{T}$ is defined by

$$\tilde{T} \equiv \frac{\omega_e^2}{4\omega_s^2} \left(\frac{E_T^2}{8\pi\, n_e T_e} \right),$$

so that $\tilde{K}/\tilde{T}$ gives directly the ratio of energy densities in the pump and daughter waves. In Eq.(5.6) we have also neglected the convective transport of TE waves out of the source region, because its rate is small compared to γ_d. Equation (5.7) has the solution

$$\tilde{K}(t) = \tilde{K}_o + \tilde{T}_o - \tilde{T}(t),$$

where subscript zero denotes initial value at the beginning of the decay. Substituting this into Eq.(5.6), we may solve for $\tilde{T}(t)$ in quadrature:

$$\omega_e\, t = 2 \times 10^3 \, \frac{\eta^{1/3}}{\xi^2} \, \frac{1}{\tilde{K}_o + \tilde{T}_o} \, \ell n \left[\frac{\tilde{T}/\tilde{T}_o}{1 + \frac{\tilde{T}_o}{\tilde{K}_o} - \frac{\tilde{T}}{\tilde{K}_o}} \right] \tag{5.8}$$

Then denoting by $\bar{t}$ the time at which $\tilde{T} = \tilde{K}_o$, we find (using $\tilde{T}_o << \tilde{K}_o$)

$$\omega_e\, \bar{t} \simeq 4 \times 10^3 \, \frac{\eta^{1/3}}{\xi^2 \tilde{K}_o} \, \ell n \left(\frac{\tilde{K}_o}{\tilde{T}_o} \right) . \tag{5.9}$$

Assuming that the initial noise level in TE modes is of the same order of magnitude as that in electrostatic modes, we may employ the arguments of Appendix C to estimate

$$\frac{\tilde{K}_o}{\tilde{T}_o} \simeq \frac{n\, N_D}{\xi^7} \simeq N_D \simeq 10^8 ,$$

where we replace η/ξ^7 by unity because the dependence on this factor is only logarithmic. Furthermore, taking the initial pump level to be given by K_{sat}, we have $\tilde{K}_o \simeq \eta^{4/3}/4\mu\xi^4$, where $\mu = 1/1836$ is the electron-to-proton mass ratio. Defining ε by $\xi = 0.1\,\varepsilon$, with ε of order unity, we finally obtain $\omega_e \bar{t} \simeq \varepsilon^2/5\eta$, so that

$$\bar{t} \simeq \frac{3 \times 10^{-8}\, \varepsilon^2}{\eta\, f(\mathrm{MHz})} \quad (\mathrm{s}) \,. \tag{5.10}$$

Thus, for $10^{-8} < \eta < 10^{-7}$, the duration of the decay phase at 30 MHz is between 0.1s and 1s, in excellent accord with the observed burst durations.

As a further test, we note that because the decay duration $\bar{t}$ is less than or of the order of the observed duration of elementary bursts, the source dimension D_s is essentially limited to being less than or of the order of the distance traversed by a wave of group velocity $V_g = \alpha_T c$ in the observed duration. Taking $\alpha_T \sim 0.20$, we find $D_s \simeq 0.08\ R_\odot$ if the observed duration is 1s. This is an apparent size of 1.3 arc min, consistent with the apparent sizes of type III burst sources (Palmer and Lin 1973).

5. Polarization

In the decay instability described in IV, the daughter TE wave has its electric vector along the electric vector of the pump wave, which in turn is approximately parallel to the magnetic field, which guides the beam. Thus the TE wave is emitted at large angles to the local magnetic field, as indicated by observations (see §I), and is linearly or highly elliptically polarized. Any circular polarization observed in elementary bursts must thus be mostly impressed upon the waves during their propagation through the corona. Because all the striations in a single given elementary burst group originate in the same source volume, they follow the same ray paths and thus will exhibit the same sense and degree

of limiting polarization. Each elementary burst in a chain, however, originates in a different volume and so the limiting polarizations may vary among elementary burst groups, which traverse different ray paths.

6. Energetics

As discussed above, type IIIb bursts are beamed mainly at large angles to the local magnetic field. Therefore, knowing the source-region diameter D_s, we can estimate the energy requirement by considering the power flow across the sides of a cylinder. The received power is

$$P = W \frac{\pi D_s \delta r}{r^2} V_g \text{ (erg cm}^{-2} \text{ s}^{-1}), \tag{5.11}$$

where r is the distance from the source to the observer, δr is the radial dimension of the source region, and W is the energy density of TEM waves. For a single striation $\delta r \simeq \frac{\Delta f}{f} L$; using Newkirk's active streamer model (fig. 9), we have $L \simeq .5\ R_\odot$ at 30 MHz, and $\delta r \simeq 1.5 \times 10^{-3}\ R_\odot$. Thus, taking $V_g = 0.1\ c$, $r = 215\ R_\odot$, and $D_s = 0.08\ R_\odot$ in accord with our previous estimates, we obtain

$$P \simeq 20\ W \text{ erg cm}^{-2} \text{ s}^{-1}.$$

From the arguments above, where we calculated $\bar{t}$, we see that W should be taken as the saturated energy density of the pump waves. Thus

$$P \simeq 20 \frac{\eta^{4/3}}{\xi^2} n_e T_e \text{ erg cm}^{-1} \text{ s}^{-1}.$$

Taking $n_e = 10^7$ ($f \simeq 30$ MHz), $T_e = 2 \times 10^6$ K, we get finally

$$P \simeq 7 \times 10^{-2} \frac{\eta^{4/3}}{\xi^2} \text{ erg cm}^{-2} \text{ s}^{-1}. \tag{5.12}$$

The received intensity of type III emission at decameter frequencies is typically of order 10^{-15} erg cm^{-2} s^{-1} Hz^{-1}, and in a bandwidth of 100 kHz

this becomes 10^{-10} erg cm^{-2} s^{-1}. Type IIIb bursts are characteristically one to ten times as bright as the following type III emission. Thus from (5.12), we require

$$\frac{\eta^{4/3}}{\xi^2} \gtrsim 10^{-9}\,\alpha,$$

where $1 \lesssim \alpha \lesssim 10$. Taking $0.05 \lesssim \xi \lesssim 0.1$ and $\alpha \simeq 10$, this becomes

$$\eta^{4/3} \gtrsim 2 \times 10^{-11} - 10^{-10},$$

or

$$\eta \gtrsim (1\text{-}3) \times 10^{-8},$$

in excellent accord with the values of η required by the other facets of the theory.

7. Drift Rate

In § I it was mentioned that in a very few cases, elementary bursts were observed to drift in frequency with rates $|\dot{f}| \lesssim 150$ kHz s^{-1}. the average rate being $\simeq -18$ kHz s^{-1} (de la Noë 1975). Such frequency drifts are unusual and are not intrinsic to the simple theory we have formulated here. On the other hand, the fact that 99.8% of the observed drifts are negative indicates that when they occur, they are a systematic effect. One possibility is that such frequency drifts may be accounted for in a more detailed kinetic treatment of the theory that does not completely separate the time scales for the various instabilities. Another possibility which fits naturally into the context of our theory, is that the frequency drifts are due to variability in the source region itself.

To see this, we note that for the daughter TE waves, the group velocity $V_g = \alpha_T c$; from Figure 6 we can see that α_T is independent of η -- and therefore of either n_e or n_b -- and depends only on $V = V_e/V_\phi$. From Eq. (5.2) we see that the α_T-dependence of a striation group depends on $V_o \equiv V_e/U$. Therefore

variations in either the electron temperature or the beam velocity across the source region will lead to slight variations in the refractive indices -- and therefore the frequencies and group velocities -- of the daughter waves. (We note, however, that these variations are not sufficient to mix the different elements of a striation group.)

Consider then the following simplified model of ray propagation in and near the source region. The refractive index goes to unity over a distance S which we expect to be roughly comparable to a density-gradient scale length L. We assume that all the waves propagate in one direction at near their initial group velocity, to the "cross-over" point S, after which they propagate at $V_g \sim c$. If $S >> D_s$, we may neglect the variation of position within the source region, and all the waves travel essentially the same distance. The time for a ray with frequency f and group velocity V_g to reach S is given by $t(f) = S/V_g$. Then the frequency drift measured by an observer at (or beyond) S is

$$\frac{df}{dt} = \frac{-V_g^2}{S\, dV_g/df} \simeq \frac{-\alpha_T^3 c}{S} f ,$$

where we have used $V_g = \alpha_T c$ and $2\pi f = \omega_e (1 + \alpha_T^2/2)$. To estimate whether this is a reasonable model, we set f = 30 MHz, df/dt ≈ -30 kHz s^{-1}, so that

$$\alpha_T^3 \frac{\alpha}{S} \simeq 10^{-3}\ s^{-1} .$$

Then for $0.1 \lesssim \alpha \lesssim 0.2$, we find $3 \times 10^{10} \lesssim S \lesssim 2 \times 10^{11}$ cm, in reasonable agreement with the assumption $D_s \sim 0.1\, R_0 << S$ and $S \gtrsim L$. The few cases (≈0.2%) in which df/dt is positive may be attributed to instances in which either D_s is abnormally large or S abnormally small, so that $D_s \sim S$ and variations of the path lengths to the cross-over region become important:

then source regions producing lower-group-velocity waves may be closer to the "cross-over" region.

Finally, we may estimate the order of magnitude of the source fluctuations necessary to produce the observed drift rates according to this model. The indicated total variability in frequency across the source is given by

$$\frac{\Delta f}{f} \simeq \frac{1}{f}\left|\frac{df}{dt}\right| \bar{t},$$

where $\bar{t}$ is, as above, the burst duration. But $2\pi f = \omega_e\ (1 + \alpha_T^2/2)$, and so

$$\frac{\Delta f}{f} \simeq \alpha\Delta\alpha \simeq \alpha \frac{d\alpha_T}{d\xi}\ \Delta\xi.$$

Taking $\alpha \simeq \xi \simeq 0.1$, we have $d\alpha_T/d\xi \simeq 2$ (c.f. Figure 6), and $\Delta\xi \sim \xi\ \Delta T_e/T_e$ if the variation is owing to temperature fluctuations, while $\Delta\xi \sim \xi\Delta U/U$ owing to variations in the beam velocity. In either case, fluctuations of $\lesssim$ 1-10% across the source region may account for drift rates of the order observed.

B. Chains of Elementary Bursts

The above exposition has concentrated on the properties of elementary bursts. We now consider the reasons why many such burst groups may occur sequentially at discrete frequencies, more or less widely spaced, to form the chain that we designate as the type IIIb burst.

Again we return to inequality (1.1), which is the fundamental condition that must be satisfied in order that our mechanism may work. Above, in considering the frequency separation between striations in an elementary burst group, we found that density ratios of order $10^{-8} \lesssim \eta \lesssim 10^{-7}$ were indicated by the observations. We now show that ratios of this order are in fact necessary in order that the linear instability discussed in §II be driven to saturation.

The linear instability may, of course, be initiated by beams with $\eta << 10^{-8}$, provided (1.1) is satisfied. Indeed, for collision frequencies $\nu_c \sim 10^{-8}\ \omega_e$, we may have $\gamma_b \gtrsim \nu_c$ for η as small as 10^{-24}. Waves are unstable, however, at phase velocities in a narrow interval slightly below the instantaneous beam velocity U(t). In this velocity interval, the beam distribution function is either zero or rising to its peak at U. Therefore, in order that the unstable waves may be driven to saturation, we require that the evolution of the beam through this velocity interval take longer than the wave growth time $N_{sat}\ \gamma_b^{-1}$. For injection at $x=0$, the time at $x > 0$ over which the beam evolves from a peak velocity U to a peak at $U-\Delta U$ is given by

$$(\Delta t)_{beam} \simeq \frac{x}{U}\left(\frac{\Delta U}{U}\right) .$$

Setting $\Delta U = V_b = \eta^{1/3} U$, we then require

$$\frac{(\Delta t)_{beam}}{(\Delta t)_{sat}} \simeq \frac{\eta^{1/3}\ x/U}{N_{sat}/\eta^{1/3}\ \omega_e} = \frac{\eta^{2/3}\ \omega_e\ x}{N_{sat}\ U} >> 1. \qquad (5.13)$$

Evaluating (5.13) at typical parameters of $\omega_e = 2 \times 10^8\ s^{-1}$ (f - 30 mHz), $x \simeq 0.6\ R_\odot$, $U = 0.5\ c$, and $N_{sat} \simeq 10$, we find $\eta >> 10^{-9}$. As soon as the beam distribution simultaneously satisfies inequalities (5.13) and (1.1), however, the mechanism should begin to operate. Thus, allowing for variations in the coronal density model, inequality (5.13) is in accord with the values $10^{-8} \lesssim \eta \lesssim 10^{-7}$ inferred earlier.

Because the beam density builds up gradually at any point r, while the ambient coronal density decreases sharply with altitude, there is some

minimum radius r_o at which inequalities (5.13) and (1.1) are first satisfied simultaneously. Of course, owing to variations in both the coronal density structure and the beam velocity profile, r_o may vary from event to event. Let us consider, however, what happens to the beam at r_o during the production of the first elementary burst.

The energy of the trapping wave, given by Eq. (2.14), is derived at the expense of the beam particles. As a consequence, the particles spread in velocity by an amount $\Delta v \simeq \eta^{1/3} U$ (Drummond et al. 1970). In the single-wave theory, which does not consider the generation of sidebands, the beam and the wave exchange energy on the time scale ω_B^{-1}, so that the beam is sequentially reconstituted with a narrow velocity spread $V_b < \eta^{1/3}U$ and then spread again, the process repeating once every bounce time (O'Neil et al. 1971). With the growth of the sidebands, however, the beam particles are untrapped, because the beat frequency between the sidebands and the main wave is $\simeq \omega_B$. This untrapping must occur over at least one bounce period, and so after the particles are untrapped their thermal spread V_b is of order Δv; i.e., $V_b \simeq \eta^{1/3}U$. Then inequality (1.1) is no longer satisfied; the beam distribution will be as schematically depicted in Figure 11-b.

Let us assume that the beam is released from the trapping wave at the point r_o and at time t_o; $t = 0$ denotes the beginning of injection. Although it is not strictly necessary to do so, we assume that injection is still occurring at time t_o. As long as injection is still occurring, the presence of particles of velocity v at a point r means that particles with velocity $v' > v$ are also at r, having been injected at times later than the injection time of the v-particles. On the other hand, at the head of

the beam the peak velocity U increases with increasing r. Consider the released beam (Figure 11). Owing to the velocity dispersion in the beam, at a point $r > r_o$ the particles at velocity U will again form the peak of the distribution function at the time $t - (r-r_{inj})/U$, where r_{inj} is the injection level. At r, however, the beam will again be narrower in velocity space than at r_o, because the slower particles at r_o have not yet evolved to r and the faster particles present at (r,t) reflect the injected distribution, not the broadened one. We now ask: what is the minimum distance r, at which another elementary burst may be produced, and how many such bursts may occur in a chain?

Assume for the moment that $\eta(r_1) \simeq \eta(r_o)$; this assumption is examined below. Then the requirement (1.1) must be satisfied at r_1 for a time of the order of t_{sb}, the time required to saturate the sidebands. In Appendix A, we find $10^{-5} \lesssim t_{sb} \lesssim 10^{-4}$ s. Thus we require that the velocity-broadened particles at $v < U$ not evolve to r_1 in the time t_{sb}, this gives

$$t_{sb} < \Delta r\, \eta^{1/3}/U, \tag{5.14}$$

where $\Delta r = r_1 - r_o$. Then the frequency separation $(\Delta f)_e$ between the elementary bursts at r_1, r_o is approximately given by

$$\frac{(\Delta f)_e}{f(r_o)} \simeq \frac{1}{\omega_e}\left|\frac{d\omega_e}{dr}\right| \Delta r \gtrsim \frac{Ut_{sb}}{2L\eta^{1/3}} . \tag{5.15}$$

Evaluating (5.15) with $\eta \sim 10^{-7}$, $U \simeq 0.5c$, $L \simeq 0.4\ R_\odot$ and $10^{-5} \lesssim t_{sb} \lesssim 10^{-4}$ s, we find

$$5 \times 10^{-4} \lesssim \frac{(\Delta f)_e}{f(r_o)} \lesssim 5 \times 10^{-3} . \tag{5.16}$$

The range (5.16) is in general agreement with observations, although frequently the elementary bursts may occur so close together in frequency that the chain appears to be a continuous burst with frequency-modulated intensity. The parameters used to evaluate (5.16), however, vary widely and so (5.16) is to be taken merely as a general estimate.

We turn now to the second question: how many elementary bursts may occur in a chain?

Consider first the radial density profile of the corona. In Figure 12 we illustrate the three density models mentioned above, for which the scale lengths L and intrinsic optical depths τ_o were calculated earlier. For the sake of definiteness, let us consider the intermediate model by Riddle (1974) which is given by

$$n_e(\rho) = \left(\frac{400}{\rho^{10}} + \frac{300}{\rho^{6}} + \frac{1}{\rho^{2}} \right) \times 10^{6} \quad \text{cm}^{-3}, \tag{5.17}$$

where $\rho \equiv r/R_\odot$ is the normalized heliocentric distance. The decameter range 20-80 mHz lies between $\rho \simeq 1.3$ and $\rho \simeq 2.0$. At $\rho = 1.3$ the terms in ρ^{-6} and ρ^{-10} are in the ratio 3:1, respectively; at $\rho = 2.0$ the term in ρ^{-6} dominates by a factor of 12. Thus we may represent the coronal density in this region by

$$n_e = n_{eo} \left(\frac{\rho_o}{\rho} \right)^{\alpha(\rho)}, \tag{5.18}$$

where $6 \lesssim \alpha(\rho) \lesssim 10$.

The beam, however, is being guided by the magnetic field, and so at comparable stages in the beam evolution at r_1 and r_o we expect the beam density to be given by

$$n_b(r) = n_b(r_o)\left(\frac{r_o}{r}\right)^2 . \qquad (5.19)$$

Therefore, for a given beam velocity U, the density ratio of the beam to the ambient plasma will be

$$\eta(r) = \eta(r_o)\left(\frac{r_o}{r}\right)^{2-\alpha(r)} \qquad (5.20)$$

Therefore, we see that the natural evolution will tend to make η, corresponding to a given value of U, larger the greater the distance from the injection point. On the other hand, the spreading of the beam by the trapping wave at r_o must remove some fraction of the particles from the velocity range $v \simeq U$; let us denote the relative magnitude of the distribution functions before and after spreading by

$$\lambda \equiv \frac{|F_b(U)|\text{after spreading}}{|F_b(U)|\text{before spreading}} .$$

Obviously $\lambda < 1$, but we expect it to be of order unity. Then assuming an elementary burst to have been produced at ρ_o, Eq. (5.20) will be modified at $\rho \gtrsim \rho_o$ to

$$\eta(\rho) \simeq \lambda\eta(\rho_o)\left(\frac{\rho}{\rho_o}\right)^{\alpha(\rho)-2} . \qquad (5.21)$$

As we have seen above, in order for an elementary burst to occur, the inequalities $\eta >> 10^{-9}$ and $V_b/U < \eta^{1/3}$ must simultaneously be satisfied. An estimate of the bound on the number of elementary bursts, B, given by the latter of these conditions may be inferred from (5.14) or (5.16), from which we may estimate B to be of order 1-10 over the decameter

range. Figure 13, from de la Noë and Boischot (1972), shows the observed distribution of B. It can be seen that most bursts indeed have B < 10.

An estimate based on (5.21) may be obtained by assuming $\rho \simeq 2.0$ and $\bar{\alpha} \simeq 7$, over this distance range. Then, since the beam density will be modified by approximately the factor λ in each burst, and since we require $\eta(\rho=2) \simeq \eta(\rho=1.3)$, we may estimate B from

$$\lambda^B \left(\frac{\rho}{\rho_o}\right)^{\bar{\alpha}-2} \simeq \lambda^B (1.5)^5 \simeq 1, \tag{5.22}$$

from which $B \simeq -2/\ln\lambda$. In Table 1 we show some values of B vs. λ according to (5.21). Although it is impossible to estimate λ precisely without making detailed calculations of the beam dynamics and evolution, we see that the range of observed values of B may be accounted for by quite plausible values of λ.

We stress here that we have made these estimates for a particular density model. The range of parameters associated with the various possible density models, together with the general variability of the parameters governing both the beam evolution and the instabilities, allow for correspondingly great variability among individual type IIIb bursts. Nevertheless, we see that it is indeed possible to combine the general features of the beam evolution and the theory for the elementary bursts, to explain how the burst chain may be produced.

Finally, we note that in the context of Eqs. (5.14) and (5.21), the simultaneous requirements on η and V_b/U may become difficult to satisfy simultaneously after many bursts have occurred or when the head of the beam has propagated to a region where the coronal density variation is

sufficiently slow so that $\eta(r)$ decreases, owing to velocity spreading. These considerations indicate why type IIIb bursts are not observed below about 10 MHz.

Appendix A - Injection and Space-Time Evolution of the Beam

Most type IIIb bursts occur in conjunction with decametric continuum or during storms of type III bursts at decameter wavelengths, which are associated with noise storms at meter wavelengths. This association indicates that types III and IIIb bursts in such storms occur when previously-accelerated particles escape from magnetically-confined regions to open field lines, and furthermore that this injection must be rather sharply delimited in time. The exact injection mechanism, however, is unknown.

Let us then consider the following phenomenological model for the injection and evolution of the beam in the lower corona. The model, of course, is neither unique nor compelling, but merely provides one of several possible contexts in which the assertion of inequality (1-1) is plausible.

We assume injection to take place at x=0, where the beam distribution function is taken to be of the form

$$F_b(x=0,v,t) = f_o(v)\ I(v,t). \qquad (A1)$$

We do not attempt to model an injection process that forms a Lorentzian distribution such as was assumed in § II, because that shape was used there only for its analytic convenience; as noted in § II, similar results concerning the beam-plasma instability may be found within a wide class of distributions, provided inequality (1.1) is satisfied.

It is reasonable to consider $f_o(v)$ to be a monotonically decreasing function of v. The function I(v,t), which we shall call the "injection

profile," must rise over a time much shorter than the typical duration between individual bursts in a storm, which in general may be of the order of seconds. We take for I the form (Figure 14)

$$I(v,t) = \begin{cases} 0, & t < 0 \ ; \\ \dfrac{t}{\tau(v)} \exp\left[- \left(\dfrac{t - \tau(v)}{\sigma(v)} \right)^2 \right], & 0 \le t \le \tau(v); \\ 1, & \tau(v) \le t \le \bar{\tau}(v) \ ; \\ 0, & t > \bar{\tau}(v) \ . \end{cases} \tag{A2}$$

As we shall see, the value of $\bar{\tau}(v)$ is not terribly important for consideration of the early evolution of F_b at $x > 0$, nor is the precise form of I for times $t > \tau(v)$, provided $I(v,t)$ reaches a maximum at $t = \tau(v)$.

A particularly simple class of velocity-dependent injection profiles may be obtained by choosing

$$\begin{aligned} \tau(v) &= \tau_0 \, \beta^{-a}, \\ \sigma(v) &= \sigma_0 \, \beta^{-a}, \end{aligned} \tag{A 3}$$

where $\beta \equiv v/c$ and τ_0, σ_0, a are constants. In particular, we note that I becomes velocity-independent for the choice $a = 0$. In the limit $\tau_0 \to 0$, $\sigma_0 \to 0$, I approaches the unit step function $H(t)$, and the injection is impulsive for all velocities.

Using the forms (A3), it is clear that if $F_0(v)$ is monotonically decreasing, $F_b(x,v,t)$ will be sharply peaked near the value $U(x,t) = \beta_b(x,t)c$ such that

$$t - \frac{x}{\beta_b c} = \frac{\tau_o}{\beta_b^{\bar{a}}} \quad . \tag{A4}$$

Owing to the modulated gaussian envelope of the rise of $I(\beta,t)$ and to the increase of $\sigma(\beta)$ as β decreases, the thermal width V_b of the beam satisfies

$$\begin{aligned} \frac{V_b}{c}(x,t) &< \left| \beta_b(x,t) - \beta_b(x,t - \sigma_o \beta^a) \right| \\ &\simeq \frac{\sigma_o \ \beta_b{}^{a+1} \ (x,t)}{t} \quad , \end{aligned} \tag{A5}$$

where we have taken $t \simeq x/\beta c \equiv t_c/\beta$. Then

$$\frac{V_b}{U} \lesssim \left(\frac{\sigma_o}{t_c}\right) \beta_b{}^{a+1} \quad ,$$

and inequality I-1, becomes

$$\left(\frac{\sigma_o}{t_c}\right) \beta_b^{a+1} < \eta^{1/3} \tag{A6}$$

For $\eta \simeq 10^{-8} - 10^{-7}$, this condition is fairly easily satisfied. We note that in the decameter range, $t \sim 1$ s, and σ_o must be considerably less than 1 s because the overall time scale of the injection is also $\lesssim 1$ s. Thus for the sake of illustration, let us take $(\sigma_o/\tau_o) \simeq 0.1$ and $a = 2$. Then for $\eta = 10^{-8}$, we would require $\beta \lesssim 0.3$, quite consistent with our earlier considerations in §V. Moreover, we may see that a wide range of plausible values for the parameters may be chosen to satisfy (A6).

Finally, we note that because we have used the one-dimensional formulation of the beam-plasma interaction (c.f. § II), inequality (1.1) actually applies to the projection of the distribution function on the direction of the magnetic field. Therefore, even if the beam were strictly monoenergetic, the spread in pitch angles $\Delta\theta$ would be required to satisfy

$$\Delta\theta < \eta^{1/3} \tag{A7}$$

in analogy with (1.1). Therefore, we must inquire whether pitch-angle scattering will broaden the beam in a time shorter than that required for the sidebands to grow. The mean-square pitch-angle scattering of an electron due to Coulomb collisions, after traversing a distance L in the plasma, is given by

$$\langle(\Delta\theta)^2\rangle = \left(\frac{8\pi\, n_e\, e^4}{m^2\, v^4}\ \ell n\Lambda\right) L, \tag{A8}$$

where v is the electron velocity and $\Lambda \equiv (3/2\ e^3)(T_e^{\,3}/\pi\ n_e)^{\frac{1}{2}}$. Evaluating (A8) at ω_e = 30 MHz ($n_e \simeq 10^7$) and v = 10 $V_e \simeq .2c$, we find that a path length $L \simeq 5 \times 10^{12}$ cm is necessary for a mean root-square scattering of 10^{-3} rad. Thus, providing the projected distribution function satisfies inequality (1.1) at any time, Coulomb collisions are absolutely negligible as a mechanism for invalidating the theory.

The other possible source of pitch-angle scattering is magnetic fluctuations. The effects of such scattering are somewhat difficult to

determine accurately. In the quasi-linear theory (Jokipii 1971), the pitch-angle scattering coefficient is given by

$$D_{\mu\mu} \equiv \frac{<(\Delta\mu)^2>}{\Delta\tau} = (\Lambda\varepsilon)^2 \frac{(1-\mu^2)}{|\mu|} \frac{1}{1 + (\varepsilon/\mu)^2} \tag{A9}$$

where $\varepsilon = L_B/R_e$, $\mu = \cos\theta$, and $\Lambda = (\delta B/B)_{rms}$ is the rms value of the field fluctuations. L_B is the correlation length of the field fluctuations R_e the electron gyroradius, and $\Delta\tau$ is given in correlation times: $\Delta\tau = vt/L_B$.

A precise assessment of the scattering coefficient is difficult because the parameters in (A9) are, of course, not well known very near the sun. Let us assume that the scale length L_B is $\sim 10^9$ cm, the scale length of supergranulation, and that the field strength is of order 1 gauss. Then for $v \sim .3c$, $\varepsilon \sim 10^3$, and (A9) becomes independent of ε. Writing $<(\Delta\mu)^2> \simeq (1-\mu^2)<(\Delta\theta)^2>$, taking $|\mu| \lesssim 1$, and setting $\Delta\theta \sim \eta^{1/3}$, we find the scattering time τ_{scatt} to be

$$\tau_{scatt} \simeq \frac{\eta^{2/3} L_B}{\Lambda^2 v} . \tag{A10}$$

Setting $\Lambda \sim 0.1$ (the approximate upper limit for validity of the quasi-linear theory), $v \simeq .3c$, and $\eta \simeq 3 \times 10^{-8}$, we find $\tau_{scatt} \simeq 10^{-4}$ s. Assuming ten e-foldings are necessary for saturation of both the trapping waves and the sidebands, we find $t_{growth} \simeq 20/\eta^{1/3}\omega_e \simeq 3 \times 10^{-5} - 10^{-4}$ s. Thus, within the context of this rather speculative calculation, pitch-angle scattering by magnetic irregularities may be marginally sufficient to compete with the tendency of the beam evolution to satisfy (1.1).

Appendix B – REMARKS ABOUT THE SINGLE-WAVE THEORY AND SIDEBAND INSTABILITY

The theory we have presented above invokes three distinct processes that occur sequentially on well-separated time scales: the strong beam-plasma interaction, which we have described in the context of the single-wave theory; the parametric sideband instability; and the parametric decay instability. Although each of these elements of the theory has been discussed more or less extensively in the literature, there remains some degree of contradiction between theoretical and experimental results, and our understanding of the individual processes is not yet complete. These remarks apply particularly to the sideband instability. Furthermore, to our knowledge, the sequential evolution of the three processes such as we have described above has never been observed in laboratory plasmas. Therefore, although at the least we may consider the theory merely as a model which successfully organizes the observed phenomenology of the type IIIb bursts, it seems desirable to discuss briefly the present state of evidence bearing upon the elements of the theory.

The single-wave theory was tested in a comprehensive experiment by Gentle and Lohr (1973), who verified the theory in all respects up to the time the main wave passes through one amplitude oscillation. At that time, they observed the main wave to dissipate into an incoherent turbulent spectrum, while the particle distribution function became very broad. It is implicit in our mechanism, of course, that the main wave remain coherent long enough to amplify sidebands to a significant level. Assuming that the sidebands grow to levels comparable to that of the

main wave (not necessarily a good assumption, as we shall discuss below), estimates in Appendix C indicate that of the order of ten e-folding times γ_{sb}^{-1} are required.

The reasons for the breakup of the trapping wave in the experiment of Gentle and Lohr are not well understood (K.W. Gentle, private communication), and different effects may dominate in different parameter regimes. Some possible mechanisms that may play a role, for example, are the oscillating two-stream instability and three-wave coupling. The experiment may also be influenced by gradients. In addition, it is unclear how the experimental results may scale with η. The breakup of the wave is probably not due to demodulation by the more slowly-growing waves in the initially unstable wave packet, however, for it is found both theoretically and experimentally that the saturation of the fastest-growing wave suppresses the further growth of nearby waves (DeNeef, Malmberg, and O'Neil 1973).

Gentle and Lohr did not attempt to observe sidebands. Beam-plasma experiments in which sidebands were observed were conducted by van Wakeren and Hopman (1972), Mizuno and Tanaka (1972) Jungwirth, Piffl, and Ullschmied (1974), and Nyack and Christiansen (1974). Thus, there is direct experimental evidence that sidebands may be amplified in beam-plasma interactions, the initial stages of which are described by the single-wave theory.

With regard to the sideband instability itself, however, there is general disagreement between experiments and theory and among different experiments. Existing theories may be classed as either parametric

(Kruer et al. 1969; Goldman and Berk 1971; Wong 1972) or "quasilinear" (Bud'ko, Karpman, and Shklyar 1971; Brinca 1972). In the parametric case, only the interaction between resonant electrons and a single driven mode is considered, while quasilinear theories consider the interaction with other modes during the evolution of the distribution function. There are also two general types of experiments -- those in which a beam amplifies the trapping wave, and those in which a large-amplitude wave is launched into the plasma.

Parametric theories of the instability predict growth of both upper and lower sidebands. In the quasilinear theory of Bud'ko et al., the lower sideband (with slightly faster phase velocity) dominates, while Brinca finds both upper and lower sidebands, although he argues that the faster sideband should dominate, owing to Landau damping of the slower one. Experiments, on the other hand, generally observe either one or the other sideband. van Wakeren and Hopman, Mizuno and Tanaka, and Jungwirth et al. all observe the lower sideband, while Nyack and Christiansen observe the upper one. These latter authors, however, argue that these results are consistent if the slower sideband is the unstable one, because in the experiments of van Wakeren and Hopman and Mizuno and Tanaka the linearly unstable wave is near the upper hybrid frequency and the upper sideband corresponds to the slow space-charge wave. (This comment appears to apply also to the experiment of Jungwirth et al.) The above experiments all involve beam-plasma interaction. In the launched-wave experiments of De Neef (1974) and Van Hoven and Jahns (1975), the lower (faster) sideband was observed. In both of

these experiments, however, coupling between sidebands is also observed. Jahns and Van Hoven (1975) attribute this coupling to a passive four-wave mode coupling process, thereby arguing against the parametric interpretation of the instability. Thus, whether or not the sideband instability is parametric, experiments indicate the possibility of amplification of both upper and lower sidebands.

A further discrepancy between theory and experiments arises when we consider the amplitudes of the main wave and the sidebands during the instability. In §V we assumed that the sidebands grow to amplitudes comparable to that of the main-wave saturation amplitude. This assumption does not necessarily violate conservation of energy, because the energy in the sidebands may come from the particles. In addition, all the theoretical treatments we have cited assume the main wave remains at constant amplitude. (Kruer and Dawson [1970], though, did computer simulations in which the energy of the main wave was depleted as the sidebands grew.) In both theory and experiment, however, the amplitude of the main wave oscillates over a factor of about five during the bounce period, and corresponding oscillations are observed for the sidebands. Nevertheless, this fact is not crucial to our theory, because we considered the wave amplitudes in the context of the energetic requirements of type IIIb bursts, and found in §V that for the most demanding case ($\alpha \simeq 10$) these requirements were well met. In the same vein, we note that the experimental results of Van Hoven and Jahns are that the amplitude of the main wave decreases about two orders of magnitude while the sideband grows, both waves asymptotically approaching the same amplitude. Jungwirth

et al., also found the sidebands to approach the amplitude of the main wave. Again, there appears to be no essential difficulty for the theory here, since our estimate of the energy requirements was shown to be well satisfied.

Finally, we note that the growth rate for the sideband instability that we calculated in III is $\gamma_{sb} \simeq 0.7\ \omega_B$, a value which we feel pushes against the limits of validity of the linear theory of Goldman and Berk. The experimental results of Van Hoven and Jahn and of Mizuno and Takanaka, however, indicate $\gamma_{sb} > \omega_B$.

Taken in the aggregate, these remarks show the wide divergences between theoretical and experimental results concerning the sideband instability. Part of the discrepancy doubtlessly lies in the fact that the theoretical treatments are for the case of temporal instability, while the observations are of spatial instability and include the effects of inhomogeneities, magnetic fields, and plasma boundaries. Nevertheless, it seems fair to assert that although the validity of the single-wave theory and the existence of the sideband instability are beyond doubt, a comprehensive theory of the latter is yet to be attained. In our theory of type IIIb bursts we have used the sideband instability theory of Goldman and Berk, in part because it is one of the simplest and most tractable theories extant. In addition, of course, the plasma conditions of the solar corona are much closer to the ideal conditions assumed in theoretical treatments than to the conditions of laboratory experiments, in that the corona is essentially uniform and infinite on the scales of the relevant interactions.

In this regard, we note that for the time scale of the type IIIb burst, which in §V we showed is determined by the decay rate γ_d, an experimental system such as that of Gentle and Lohr is of order ten thousand times too small to permit the sequential occurrence of the beam-plasma interaction, sideband instability, and parametric decay -- the three fundamental elements of the type IIIb burst. For this reason, we do not expect to see phenomena such as the type IIIb burst in the laboratory; the solar corona is a much more ideal plasma "laboratory" than can be created artificially.

Finally, we note that the qualitative details of our theory are relatively insensitive to the exact theory employed to describe the sideband instability, for three reasons. First, all theories predict the sidebands to be separated from the main wave by approximately the bounce frequency, and this was the essential quantitative result used in §V. Second, the time scale for the type IIIb phenomena is essentially determined by the time scale for the parametric decay instability, because this is the longest time scale in the interaction regardless of the precise growth rate of the sideband instability. Third and finally, the energetic requirements of the type IIIb bursts appear to be easily met by the theory notwithstanding the assumptions we have made regarding the amplitudes of the main and sideband waves.

Appendix C - THRESHOLD CONDITIONS FOR THE PARAMETRIC DECAY AND UP-CONVERSION INSTABILITIES

In §IV we stated, without proof, that the only parametric instability for which the threshold pump intensity is exceeded in our theory is the parametric decay instability described by Lashmore-Davies (1974a,b). In this Appendix we support this assertion by estimating the enhanced TE-wave damping rate γ_T in the source region, and computing the ratios of K_{sat} to K_c for both $\delta < 0$ and $\delta > 0$ [c.f. Eq. (4.-4)].

First, we note that the electric field of the TE wave is along the direction of the pump wave field, so that $\vec{k}_T \perp \vec{k}_L$. As we saw in §V, the magnitude $k_T = \alpha_T \omega_e/c \lesssim 0.2$. But $k_L \simeq \omega_e/U$, so that $k_T/k_L \lesssim 0.2\ U/c << 1$. Therefore, according to the resonance conditions (4.-1), $\vec{k}_S \simeq -\vec{k}_L$. This allows us to write

$$\frac{\omega_S}{\omega_e} \simeq \frac{k_S\, C_s}{k_L\, U} \simeq \frac{C_s}{U} = \mu^{\frac{1}{2}}\, \xi \ , \qquad \text{(C1)}$$

where $\mu \equiv m_e/m_p$ is the mass ratio of electrons to protons, and $C_s = \mu^{\frac{1}{2}} V_e$ is the ion sound speed. In an isothermal plasma ($T_e = T_p$), the ion sound wave is heavily damped; ignoring factors of order unity, we may take $\gamma_s \simeq \omega_s$ for the purpose of making estimates.

The damping rate γ_T in the background plasma is initially given by $\gamma_T \simeq \omega_e/2N_D$, where $N_D = n_e \lambda_e^3$ is the number of particles in a Debye sphere [$\lambda_e \equiv (T_e/4\pi\, n_e e^2)^{\frac{1}{2}}$]. However, as the decay progresses, the buildup of ion sound turbulence leads to enhanced resistivity of the plasma to waves near the plasma frequency (Dawson and Oberman 1963; Dawson 1968). Thus, the threshold K_c changes in time, and we should use the maximum

value of γ_T attainable. For an energy density W_s of sound waves, in which the typical wavenumber is k , the damping rate γ_T may be estimated (Papadopoulos 1974) as

$$\gamma_T \simeq \frac{(W_s/n_e T_e)}{k^2 \lambda_e^2} \omega_e \tag{C2}$$

Therefore, we need to estimate the maximum level of W_s.

Denote $R_o \equiv W_L/n_e T_e$, $S \equiv W_s/n_e T_e$, where W_L is the energy density of the main wave. In the wavelength interval $k_o - \delta k < k < k_o + \delta k$, the initial noise level $R_o(0)$ is given by

$$R_o(0) \simeq \frac{2}{N_D} (k_o \lambda_e)^3 \frac{\delta k}{k_o} \simeq \frac{2}{N_D} \xi^3 \eta^{1/3} , \tag{C3}$$

where to get the RHS we have used Eq. (2-10). Therefore, using Eq. (C3) and $\gamma_T(0) \simeq \omega_e/2N_D$, we have

$$\frac{K(0)}{K_c(0)} = \frac{\xi^2 \eta^{1/3}}{4 \mu^{1/2}} \simeq 10 \xi^2 \eta^{1/3} << 1. \tag{C4}$$

Using Eq. (2.14), the saturation level is

$$K_{sat} = \omega_e^2 \eta^{4/3}/4 \xi^2 . \tag{C5}$$

Denote by τ the total time the main wave takes to grow from the initial noise level to saturation. Further, we denote by τ_1 the duration between the time the wave reaches $K_c(0)$ and saturation. Then τ_1 is given by

$$\frac{K_{sat}}{K_c(0)} = \frac{N_D \eta^{4/3}}{8\mu^{\frac{1}{2}}\xi^3} \simeq \frac{5 N_D \eta^{4/3}}{\xi^3} \equiv \exp(2\gamma_b \tau_1) , \tag{C6}$$

while τ is defined, using Eqs.(C4) and (C6), by

$$\frac{K_{sat}}{K_o} = \frac{N_D \eta}{2\xi^5} \equiv \exp(2\gamma_b \tau). \tag{C7}$$

Denoting the decay rate found from Eq. (4.2) by γ_d, the sound level S_{sat} is then given by

$$S_{sat} = S(0) \exp(2\gamma_d \tau_1),$$

where $S(0) \simeq k^2 \lambda_e^2 R(0)$. Then

$$\frac{\gamma_{T,sat}}{\omega_e} = \frac{\gamma_T(0)}{\omega_e} \exp(2\gamma_d \tau_1) = \frac{2K(0)}{\omega_e^2} \left[\exp(2\gamma_b \tau_1)\right]^{\gamma_d/\gamma_b}, \tag{C8}$$

where $\gamma_b \simeq \eta^{1/3} \omega_e$ is the beam-plasma growth rate found in § II. For an overestimate, we take $\gamma_d \simeq \omega_s$; then Eq. (C8) becomes

$$\frac{\gamma_{T,sat}}{\omega_e} \simeq \frac{2K_o}{\omega_e^2} \left[\frac{5N_D \eta^{4/3}}{\xi^3}\right]^{\mu^{1/2}\xi/\eta^{1/3}}, \tag{C9}$$

where we have used Eqs. (C4) and (C6). Substituting Eq.(C9) into the first of Eqs (4.4) to determine the decay threshold at saturation, we find

$$\frac{K_{sat}}{K_{c,sat}} = \frac{N_D \eta}{16\mu^{1/2}\xi^6} \left[\frac{5N_D \eta^{4/3}}{\xi^3}\right]^{-\mu^{1/2}\xi/\eta^{1/3}}. \tag{C10}$$

K_{sat}, and $K_{sat}/K_{c,sat}$ given by (C10) are plotted in Figure 4. It is seen that under conditions of interest to our theory, K_{sat} greatly exceeds the decay threshold but is in general much smaller than the up-conversion threshold $K_{sat} = 2$.

ACKNOWLEDGMENTS

We have benefitted from informative discussions with Thomas J. Birmingham, Ronald C. Davidson, Peter De Neef, Joseph Fainberg, Kenneth W. Gentle, Melvyn L. Goldstein, John H. Malmberg, Thomas M. O'Neil, Konstantinos Papadopoulos, Hans Rosenberg, Dean F. Smith, Thomas P. Starke, Robert G. Stone, and Gerard Van Hoven. In addition, we are grateful to R.G. Stone and J. Fainberg for access to the IMP-6 and RAE-2 solar radio data. Numerical solutions of the sideband and decay dispersion relations were performed by Joseph H. Bredekamp. J.L.N. was partially supported under NASA Grants NGL 21-002-033 and NGR 21-003-367.

TABLE 1

Number of possible elementary bursts B for various values of λ: $B = -2/\ell n\ \lambda$.

λ	B
0.50	3
0.60	4
0.70	5
0.80	9
0.85	12
0.90	19
0.95	39

FIGURE CAPTIONS

Figure 1. Dynamic spectra of type IIIb bursts. (a) A type IIIb burst followed by a faint type III burst on August 8, 1970. (b) Another type IIIb burst followed by a type III burst on August 12, 1970. Vertical dotted lines are lightnings. Horizontal white lines are interferences.

Figure 2. Two-dimensional phase space in the frame moving with the phase velocity of the trapping wave.

Figure 3. (a) Maximum growth rate and corresponding wavenumber shift and real frequency shift for the sideband dispersion relation of Goldman and Berk (1971), plotted against $\xi = V_e/U$ for $\varepsilon = 2$. All quantities are normalized to ω_B.

(b) Asymptotic ($\xi \to 0$) values of the maximum sideband growth rate and corresponding frequency shift, normalized to ω_e, as a function of η.

Figure 4. (a) Saturation amplitude $\tilde{K}_{sat}$ of the main wave as a function of V, for various η.

(b) Ratio of $\tilde{K}_{sat}$ to the parametric decay threshold $\tilde{K}_{c,sat}$.

Figure 5. Maximum growth rate of the parametric decay instability, as a function of the phase velocity of the trapping wave, $V_o = \xi$. The equivalent decay rates of the sidebands may be obtained by multiplying by $(V \pm /V_o)^2$. Dashed curves--for a monochromatic pump. Solid curves--corrected for finite frequency spread in the pump.

Figure 6. Index of refraction of the TE' waves resulting from the decay of longitudinal waves at the effective normalized phase velocity V. This curve is independent of η.

Figure 7. Bandwidth of the decay wave spectrum as a function of V, for various η.

Figure 8. Effective phase velocities $V_{\pm}$ of the sidebands, as a function of V_o, for various η.

Figure 9. Scale length L of the coronal density gradient for various density models, and the corresponding intrinsic optical depths τ_o.

Figure 10. Optical depths of the decay daughter TE' waves, as a function of V_o, at 30 MHz and 100 MHz. τ_o, τ^-, and τ^+ refer to the main wave, red (lower), and blue (upper) sidebands, respectively.

Figure 11. Schematic illustration of the beam distribution function $F_b(v)$: (a) before trapping; (b) after being untrapped.

Figure 12. Coronal density models of Leblanc *et al.* (1973), Riddle (1974), and Newkirk (1967).

Figure 13. Occurrence histogram of the number N(B) of type IIIb bursts *vs* the number B of elementary bursts.

Figure 14. Schematic illustration of the injection time-modulation profile I(v,t).

REFERENCES

Aubier, M., and Boischot, A. 1972, Astron. Astrophys. 19, 343.

Brinca, A. L. 1972, J. Plasma Phys. 7, 385.

Bud'ko, N. I., Karpman, V. I., and Shklyar, D. R. 1972, Zh. Eksp. Teor. Fiz. 61, 1463 Fng. trans: Soviet Phys. JETP 34, 778 (1972) .

Dawson, J. 1968, Adv. Plasma Phys. 1, 1.

Dawson, J. and Oberman, C. 1963, Phys. Fluids 6, 394.

de la Noë, J. 1974, Solar Phys. 37, 225.
_____ 1975, Astron. Astrophys. in press.

de la Noë, J. and Boischot, A. 1972, Astron. Astrophys. 20, 55.

de la Noë, J., and Gergeley, T. 1975, in preparation.

De Neef, P. 1974, Phys. Fluids 17, 981.

De Neef, C. P., Malmberg, J. H., and O'Neil, T. M. 1973, Phys. Rev. Lett. 30, 1032.

Drummond, W. E., Malmberg, J. H., O'Neil, T. M., and Thompson, J. R. 1970, Phys. Fluids 13, 2422.

Ellis, G. R. A., and McCulloch, P. M. 1966, Nature 211, 1070.

Ellis, G. R. A., and McCulloch, P. M. 1967, Austr. J. Phys. 20, 583.

Gentle, K. W., and Lohr, J. 1973, Phys. Fluids 16, 1464.

Goldman, M. V., and Berk, H. L. 1971, Phys. Fluids 14, 801.

Johns, G., and Van Hoven, G. 1975, Phys. Fluids 18, 214.

Jokipii, J. R. 1971, Rev. Geophys. Space Sci. 9, 27.

Jungwirth, K., Piffl, V., and Ullschmied, J. 1974, Plasma Phys. 16, 283.

Kruer, W. L., and Dawson, J. M. 1970, Phys. Fluids 13, 2747.

Kruer, W. L., Dawson, J. M., and Sudan, R. N. 1969, Phys. Rev. Lett. 23, 838.

Lashmore-Davies, C.N. 1974a, Phys. Rev. Lett. 32, 289.

Lashmore-Davies, C. N. 1974b, Plasma Phys. 17, 281 (1975).

Leblanc, Y., Leroy, J. L., and Pecantet, P. 1973, Solar Phys. 31, 343.

Jokipii, J. R., 1971, Rev. Geophys. Space Sci. 9, 27.

Melrose, D. B. 1974, Solar Phys. 34, 421.

Mizuno, K., and Tanaka, S. 1972; Phys. Rev. Lett. 28, 45.

Newkirk, G. 1967, Ann. Rev. Astr. Astrophys. 5, 213.

Nishikawa, K. 1968a, J. Phys. Soc. Japan 24, 916.

Nishikawa, K. 1968b, ibid., p. 152.

Nyack, C. A., and Christiansen, P. J. 1974, Phys. Fluids 17, 2025.

O'Neil, T. M., and Malmberg, J. H. 1968, Phys. Fluids 11, 1754.

O'Neil, T. M., Winfrey, J. H. and Malmberg, J. H. 1971, Phys. Fluids 14, 1204.

Papadopoulos, K. 1974, Phys. Fluids (submitted).

Papadopoulos, K., Goldstein, M. L., and Smith, R. A. 1974, Ap. J. 190, 175.

Palmer, I.B. and Lin, R. P. 1973, in "High Energy Phenomena on the Sun" (R. Ramaty and R. G. Stone, eds.), NASA SP-342.

Riddle, A. C. 1974, Solar Phys. 35, 153.

Rosenberg, H. 1970, Astron. Astrophys. 9, 159.

Rosenberg, H. 1974, Solar Phys. (to be published).

Sanmartin, J. R. 1970, Phys. Fluids, 13, 1533.

Stewart, R. T. 1975, Solar Phys. 40, 417.

Valeo, E. J., and Oberman, C. R. 1973, Phys. Rev. Lett. 30, 1035.

Van Hoven, G., and Jahns, G. 1975, Phys. Fluids 18, 80.

van Wakeren, J.H.A., and Hopman, H. J. 1972, Phys. Rev. Lett. 28, 295.

Wharton, C. B., Malmberg, J. H., and O'Neil, T. M. 1968, Phys. Fluids 11, 1961.

Wong, H. V. 1972, Phys. Fluids 15, 632.

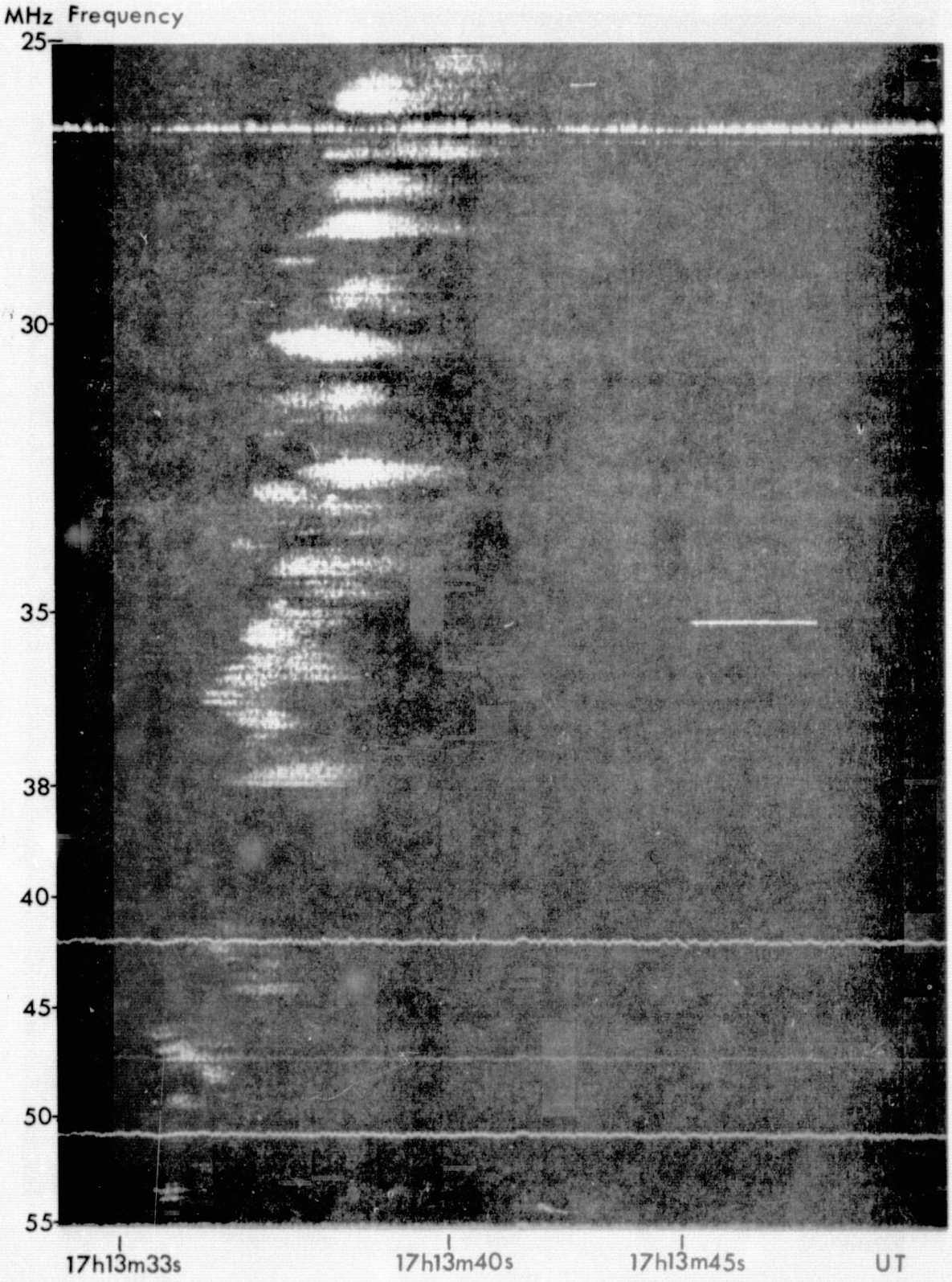

Figure 1a

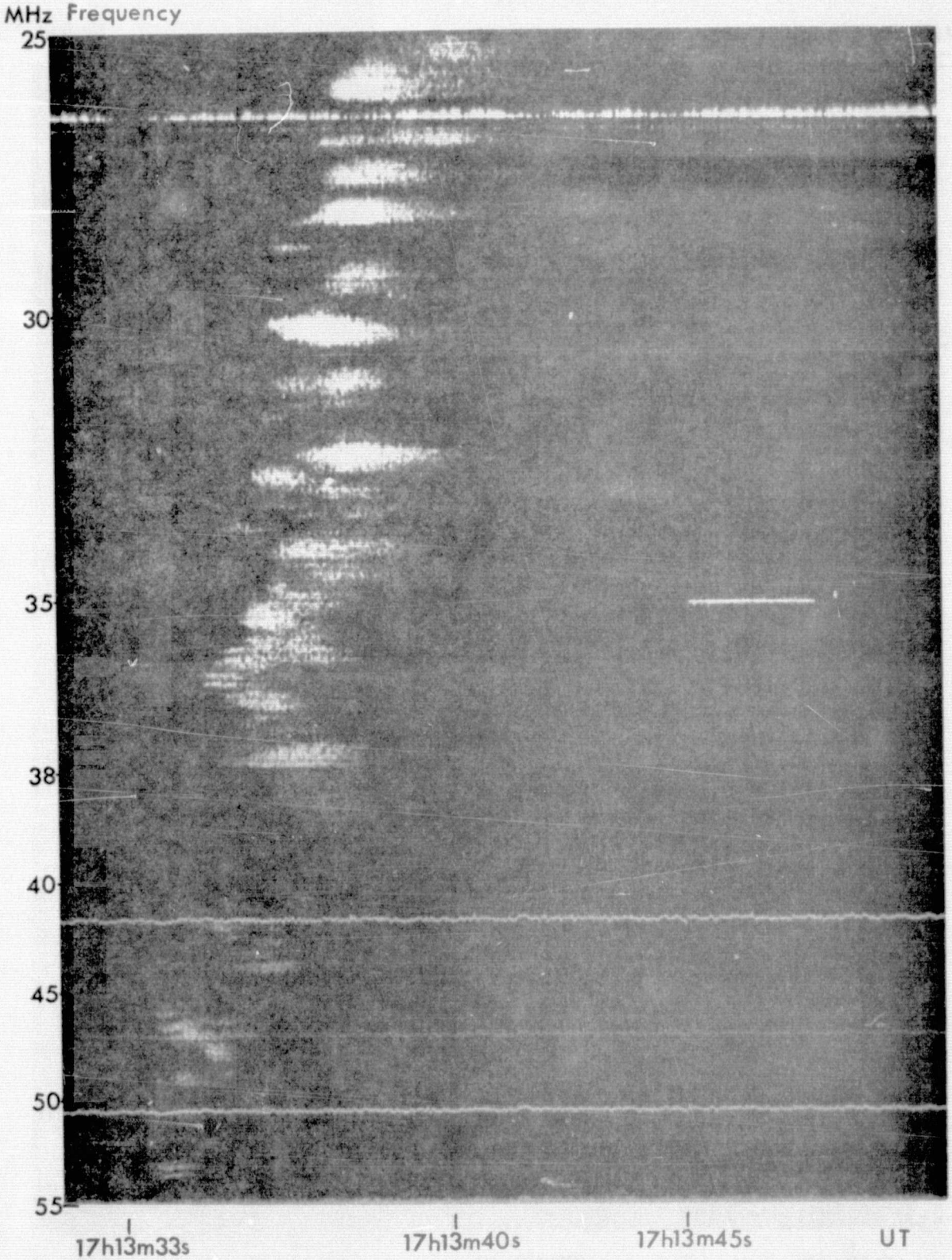
MHz Frequency
25
30
35
38
40
45
50
55
17h13m33s
17h13m40s
17h13m45s
UT

Figure 1a

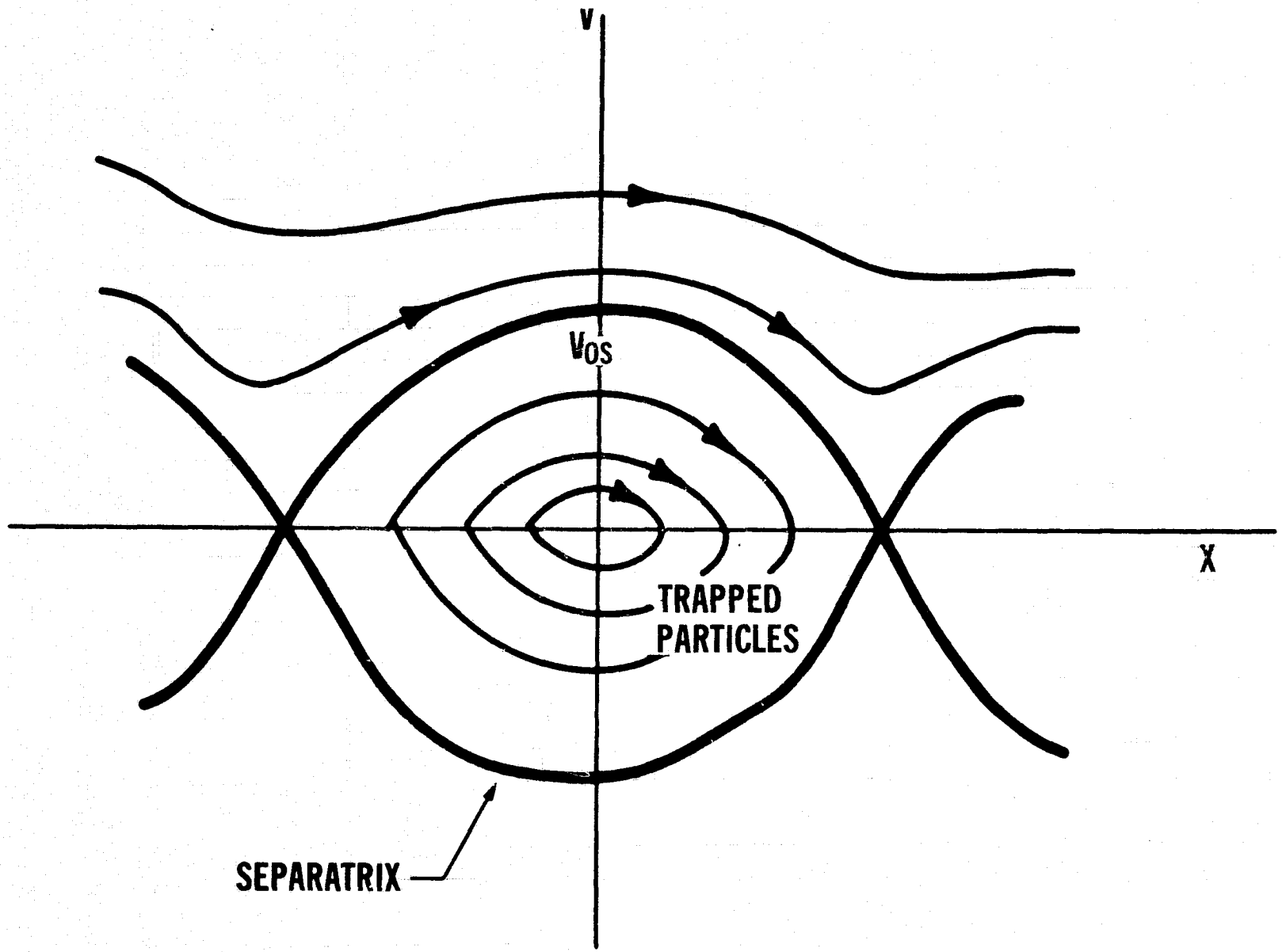

Figure 2

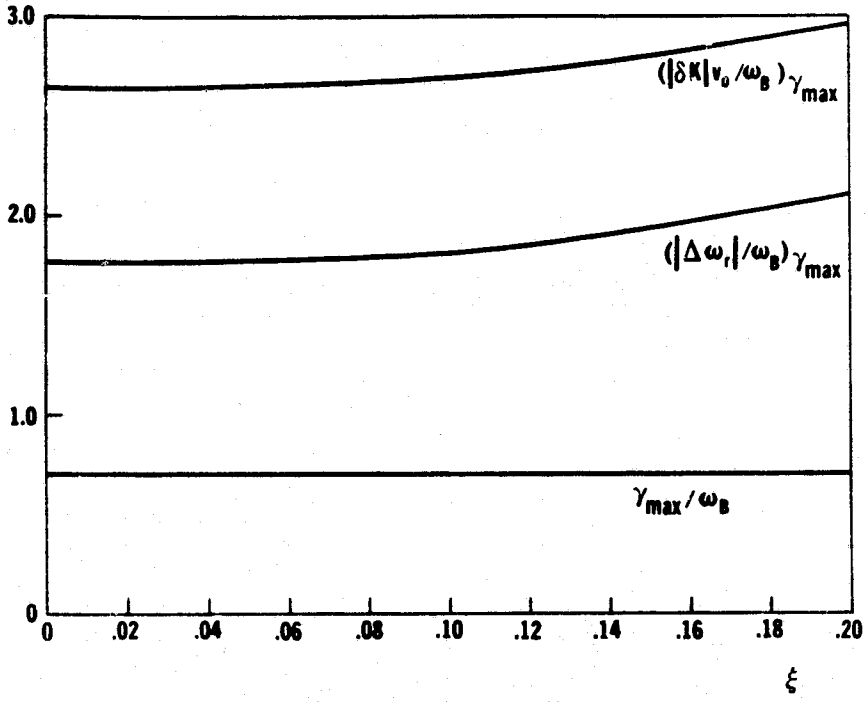
3.0
2.0
1.0
0
$(|\delta K| v_0/\omega_B)\gamma_{max}$
$(|\Delta\omega_r|/\omega_B)\gamma_{max}$
γ_{max}/ω_B
0
.02
.04
.06
.08
.10
.12
.14
.16
.18
.20
ξ

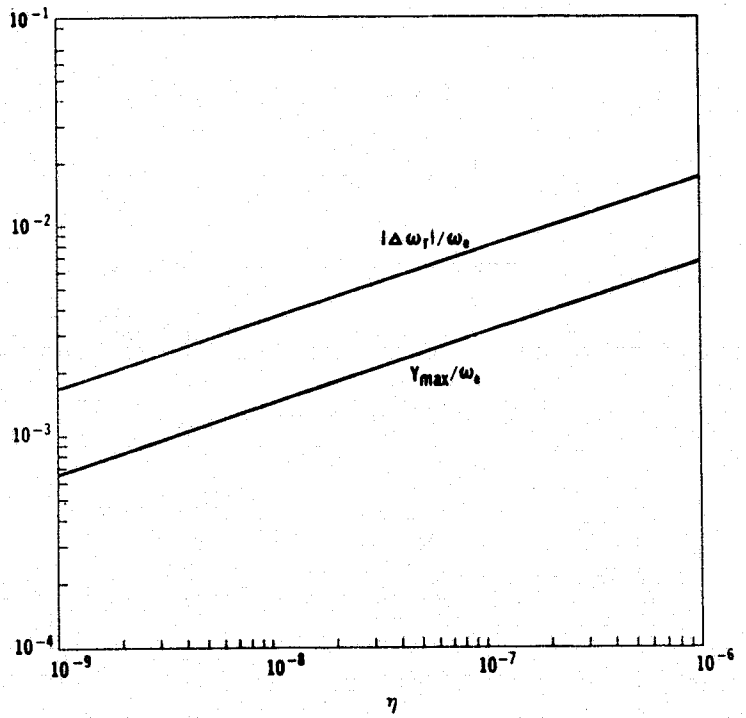
10^{-1}
10^{-2}
10^{-3}
10^{-4}
$|\Delta\omega_r|/\omega_e$
γ_{max}/ω_e
10^{-9}
10^{-8}
10^{-7}
10^{-6}
η

Figure 3a & b

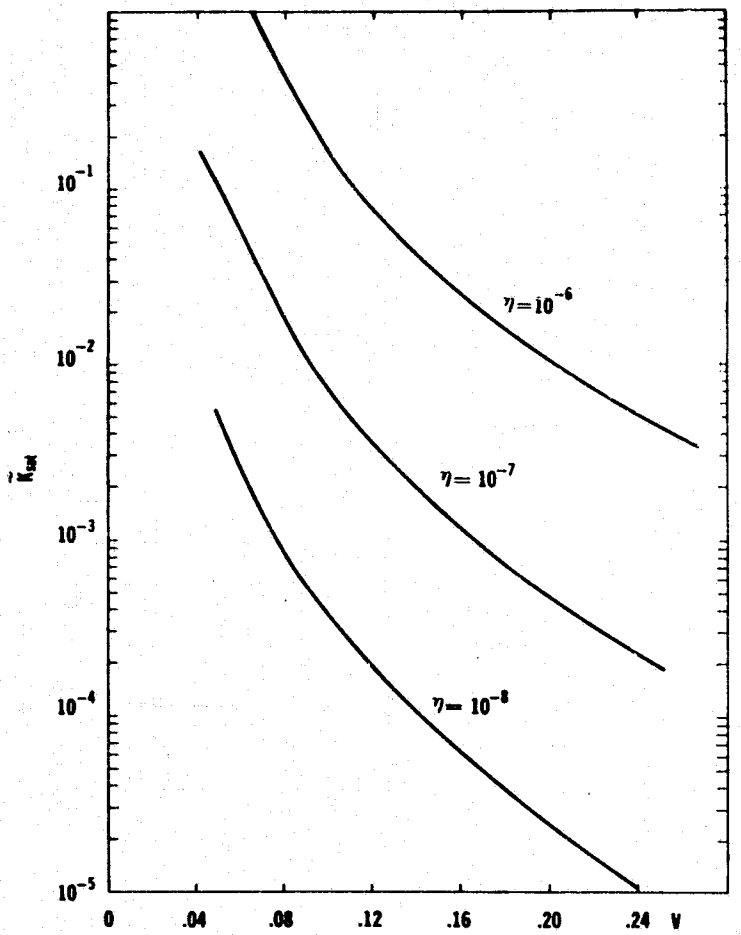
10^{-1}
10^{-2}
10^{-3}
10^{-4}
10^{-5}
$\eta = 10^{-6}$
$\eta = 10^{-7}$
$\eta = 10^{-8}$
0
.04
.08
.12
.16
.20
.24
V

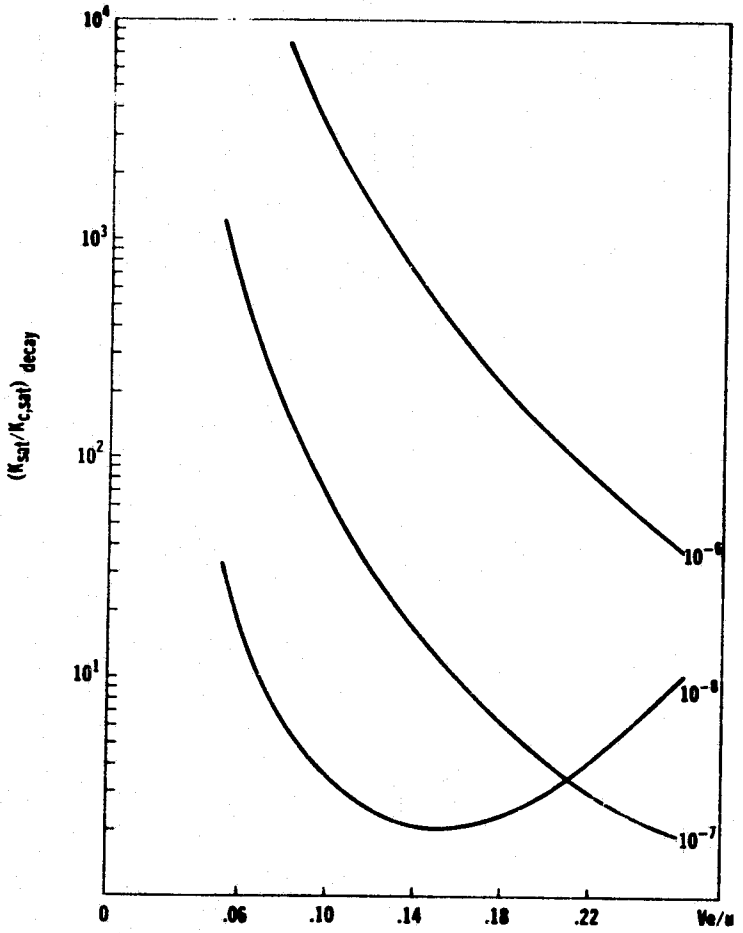
10^{4}
10^{3}
10^{2}
10^{1}
$(K_{sat}/K_{c,sat})$ decay
10^{-6}
10^{-8}
10^{-7}
0
.06
.10
.14
.18
.22
Ve/u

Figure 4a & b

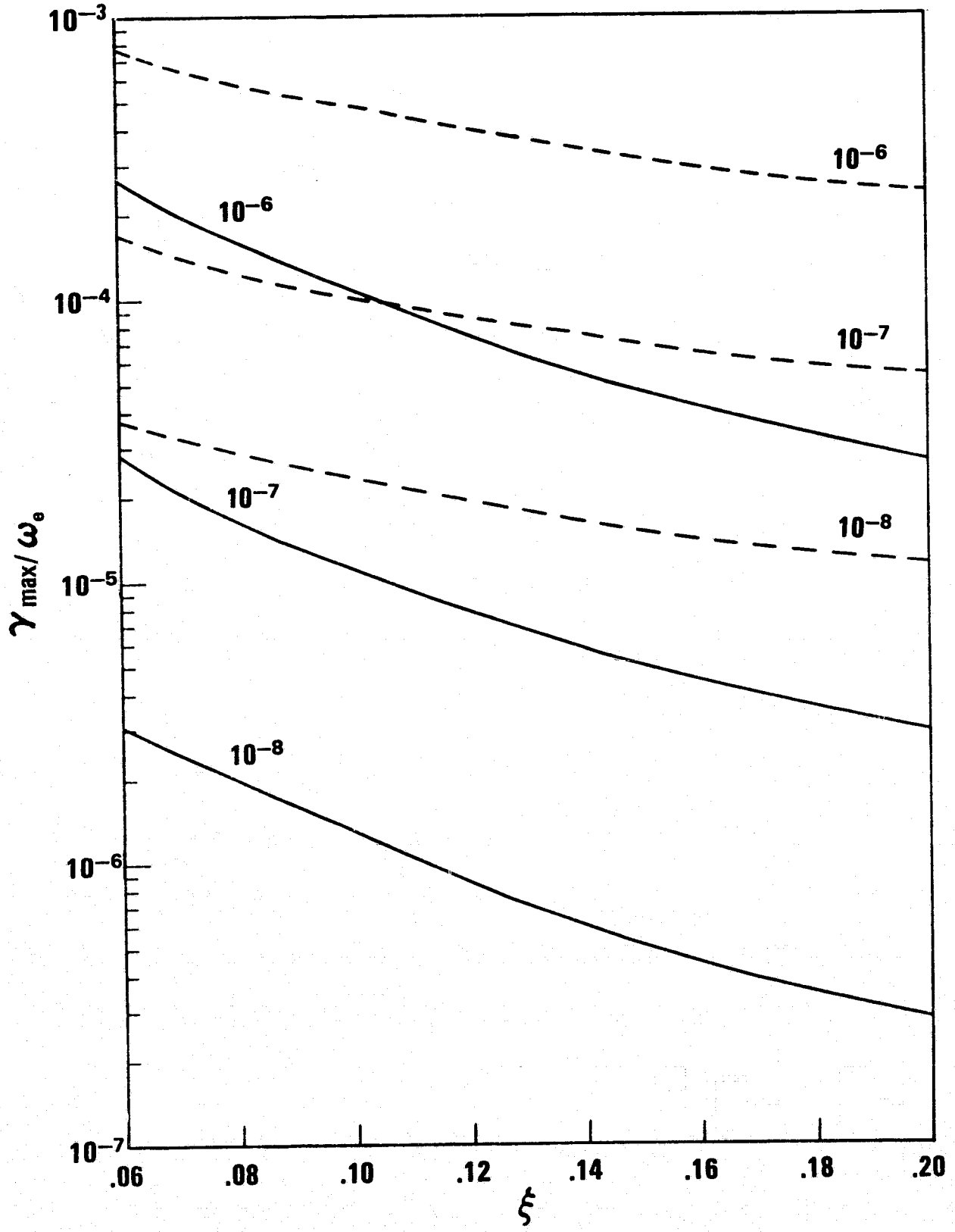
10^{-3}
10^{-4}
10^{-5}
10^{-6}
10^{-7}
γ_{max}/ω_e
10^{-6}
10^{-7}
10^{-7}
10^{-8}
10^{-8}
10^{-6}
10^{-7}
.06
.08
.10
.12
.14
.16
.18
.20
ξ

Figure 5

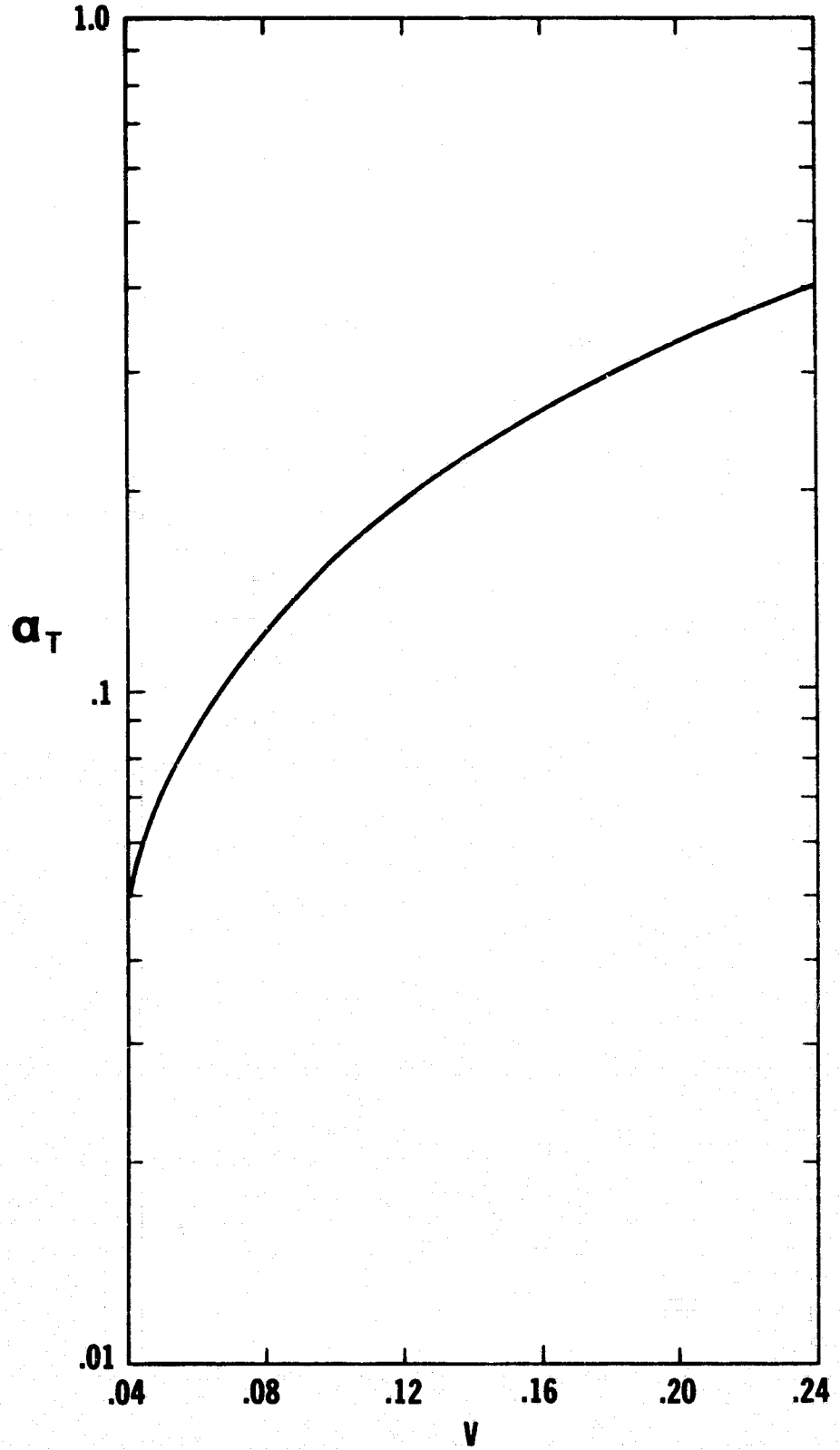

Figure 6

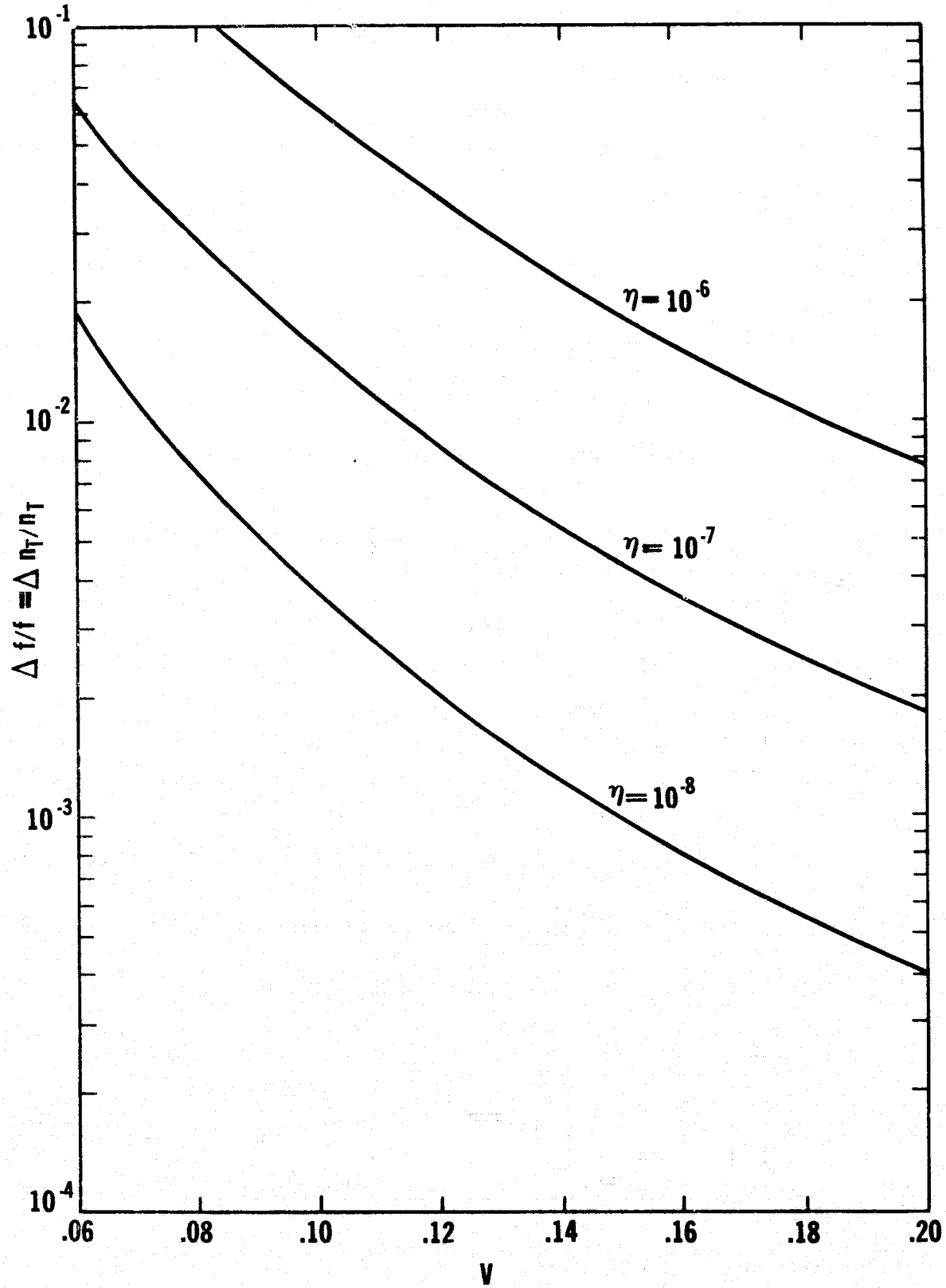
10^{-1}
10^{-2}
10^{-3}
10^{-4}
$\Delta f/f \equiv \Delta n_T/n_T$
$\eta = 10^{-6}$
$\eta = 10^{-7}$
$\eta = 10^{-8}$
.06
.08
.10
.12
.14
.16
.18
.20
V

Figure 7

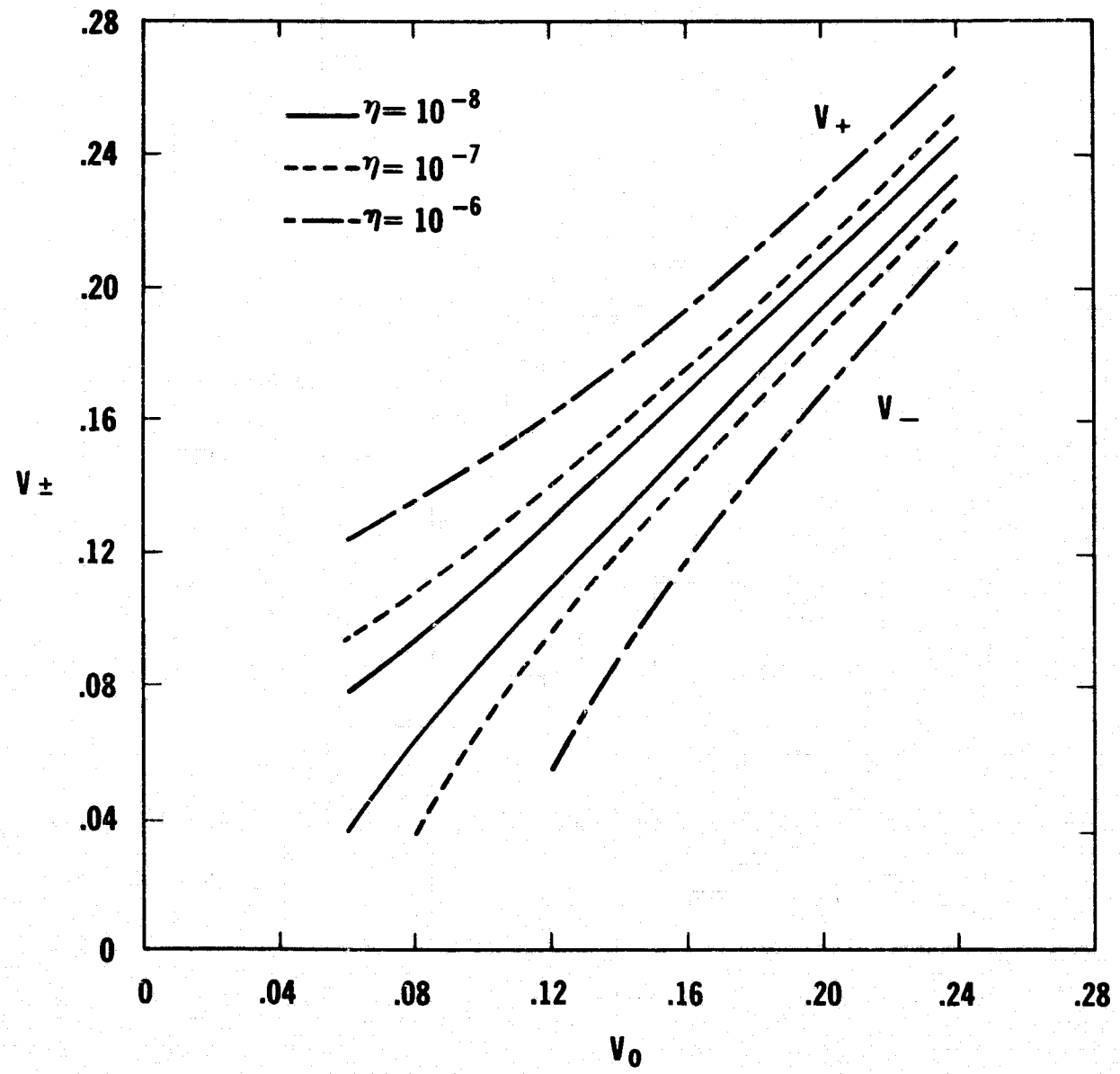
.28
.24
.20
.16
.12
.08
.04
0
V ±
$\eta = 10^{-8}$
$\eta = 10^{-7}$
$\eta = 10^{-6}$
V +
V −
0
.04
.08
.12
.16
.20
.24
.28
V_0

Figure 8

1. LEBLANC et al.
2. RIDDLE
3. NEWKIRK ACTIVE STREAMER

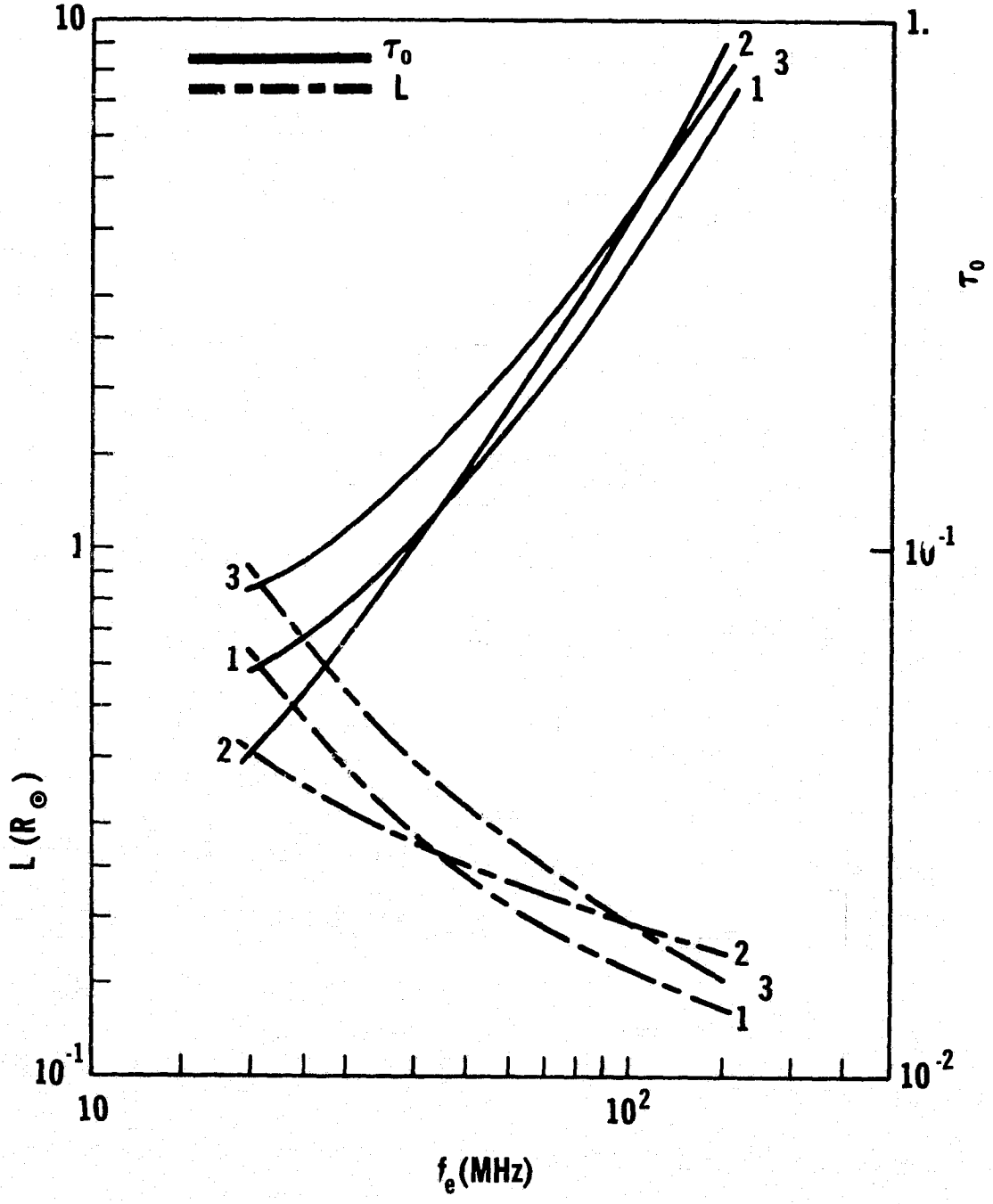

Figure 9

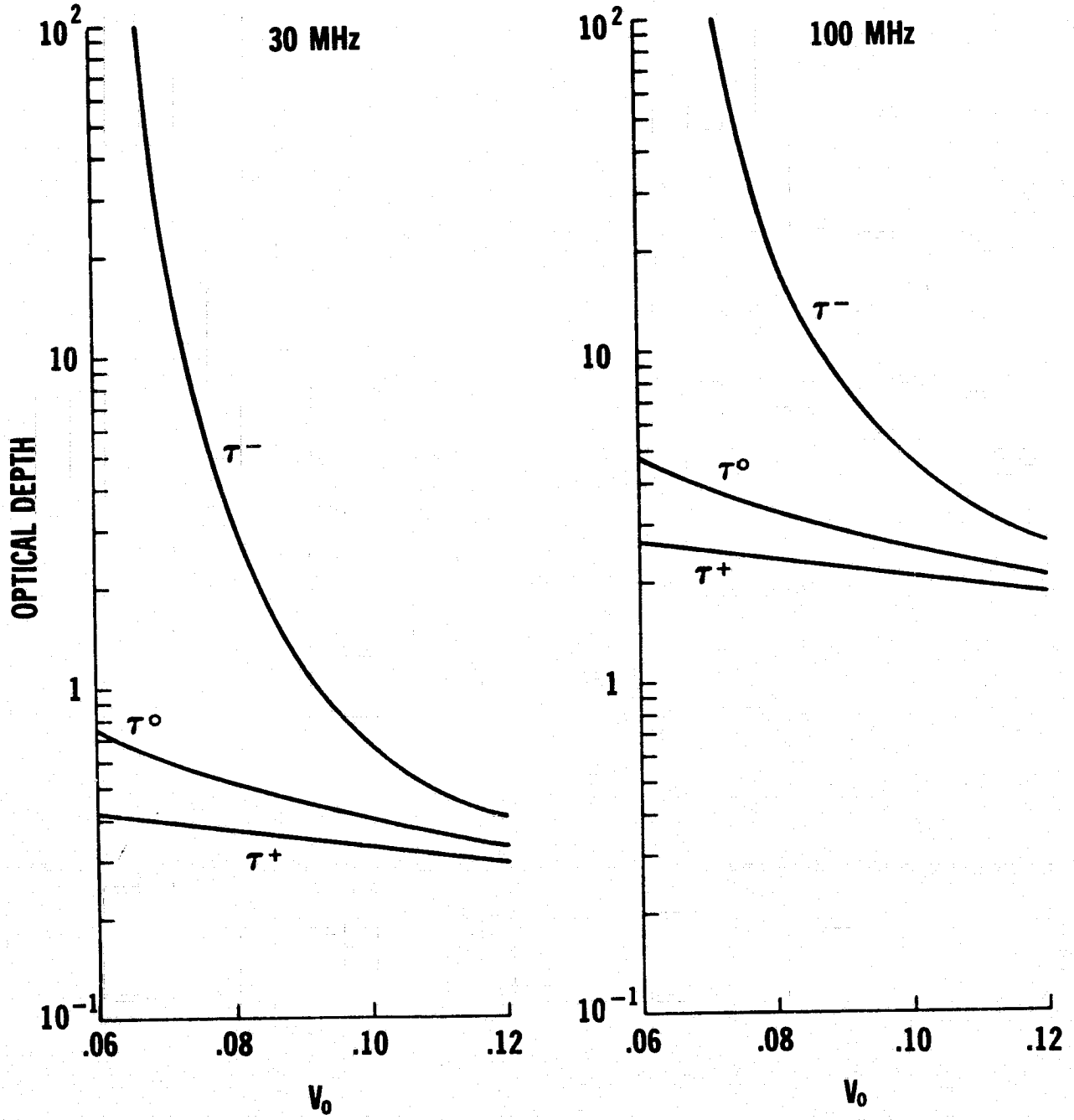
30 MHz
100 MHz
OPTICAL DEPTH
10^2
10
1
10^{-1}
τ^-
τ°
τ^+
.06
.08
.10
.12
V_0

Figure 10

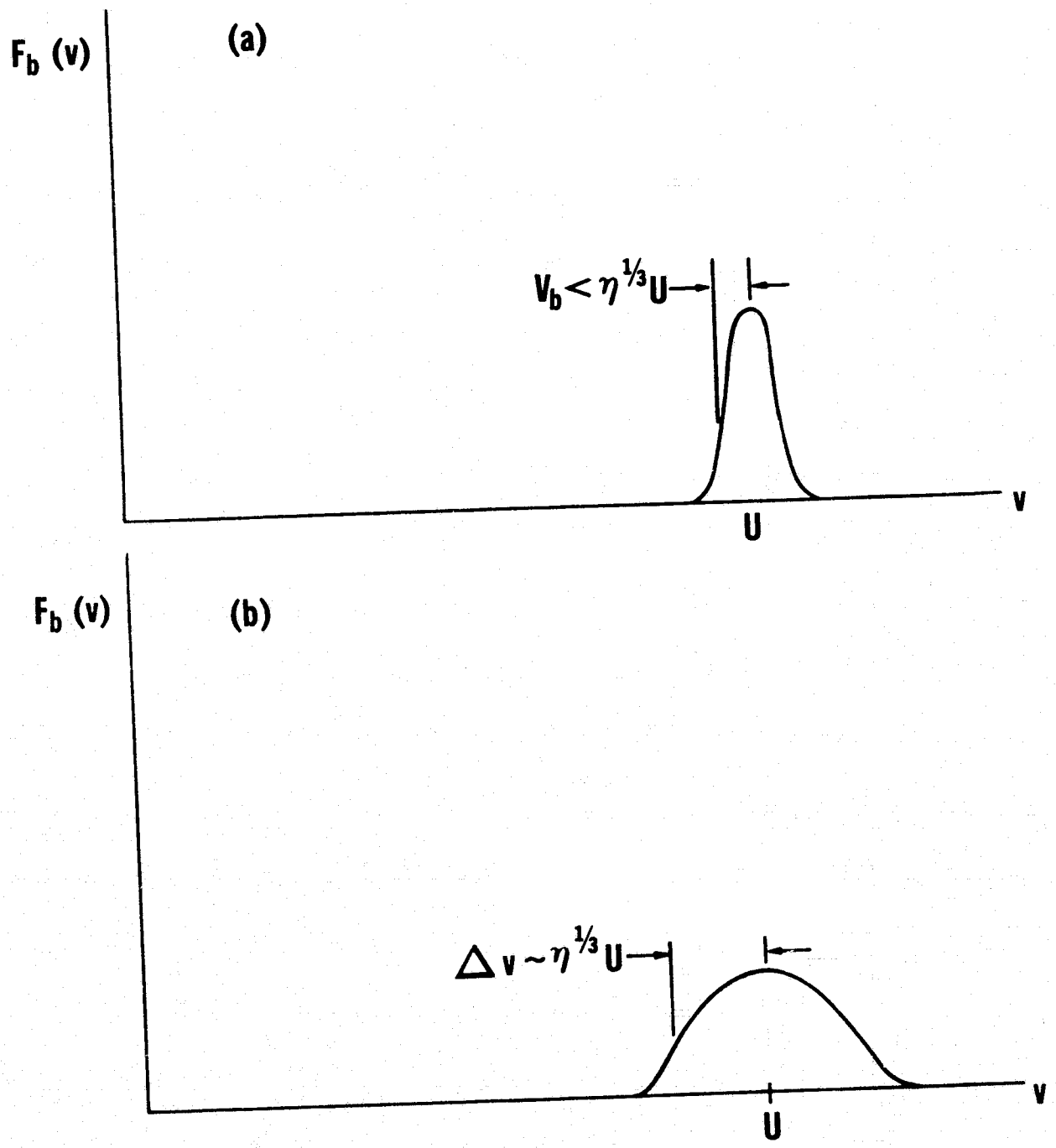

Figure 11a & b

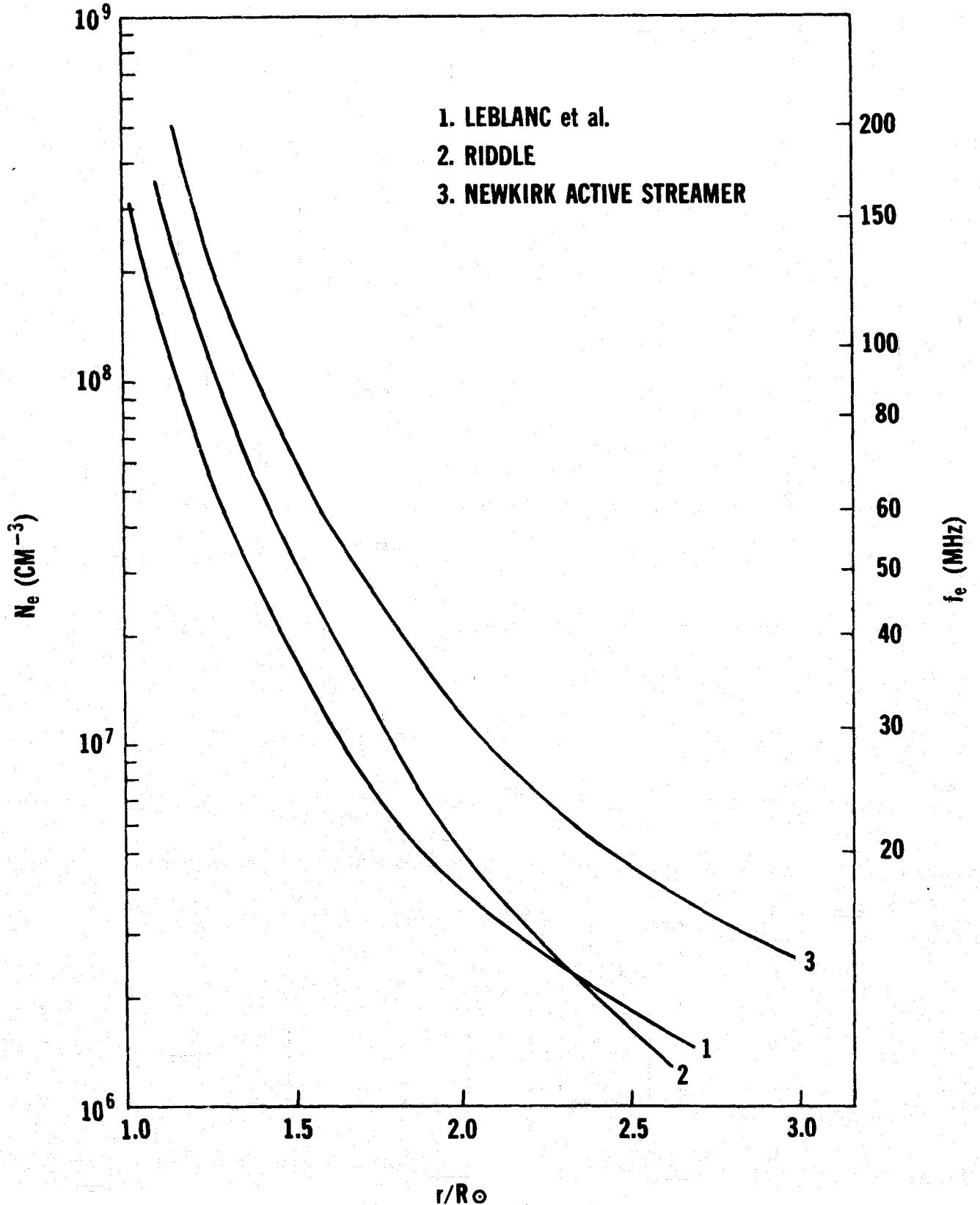
1. LEBLANC et al.
2. RIDDLE
3. NEWKIRK ACTIVE STREAMER
10^9
10^8
10^7
10^6
N_e (CM^{-3})
200
150
100
80
60
50
40
30
20
f_e (MHz)
1.0
1.5
2.0
2.5
3.0
r/R⊙
1
2
3

Figure 12

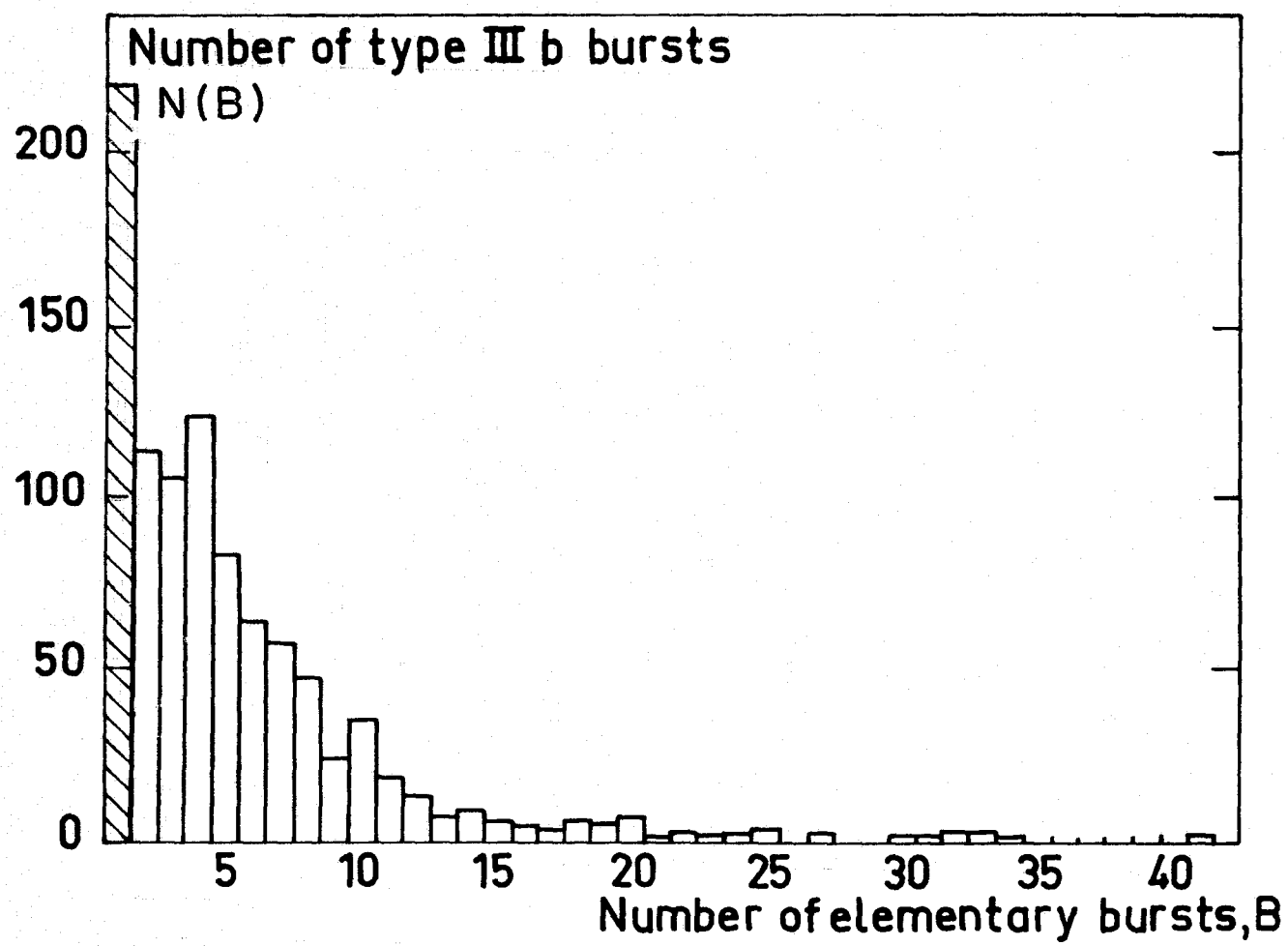
Number of type III b bursts
N(B)
200
150
100
50
0
5
10
15
20
25
30
35
40
Number of elementary bursts, B

Figure 13

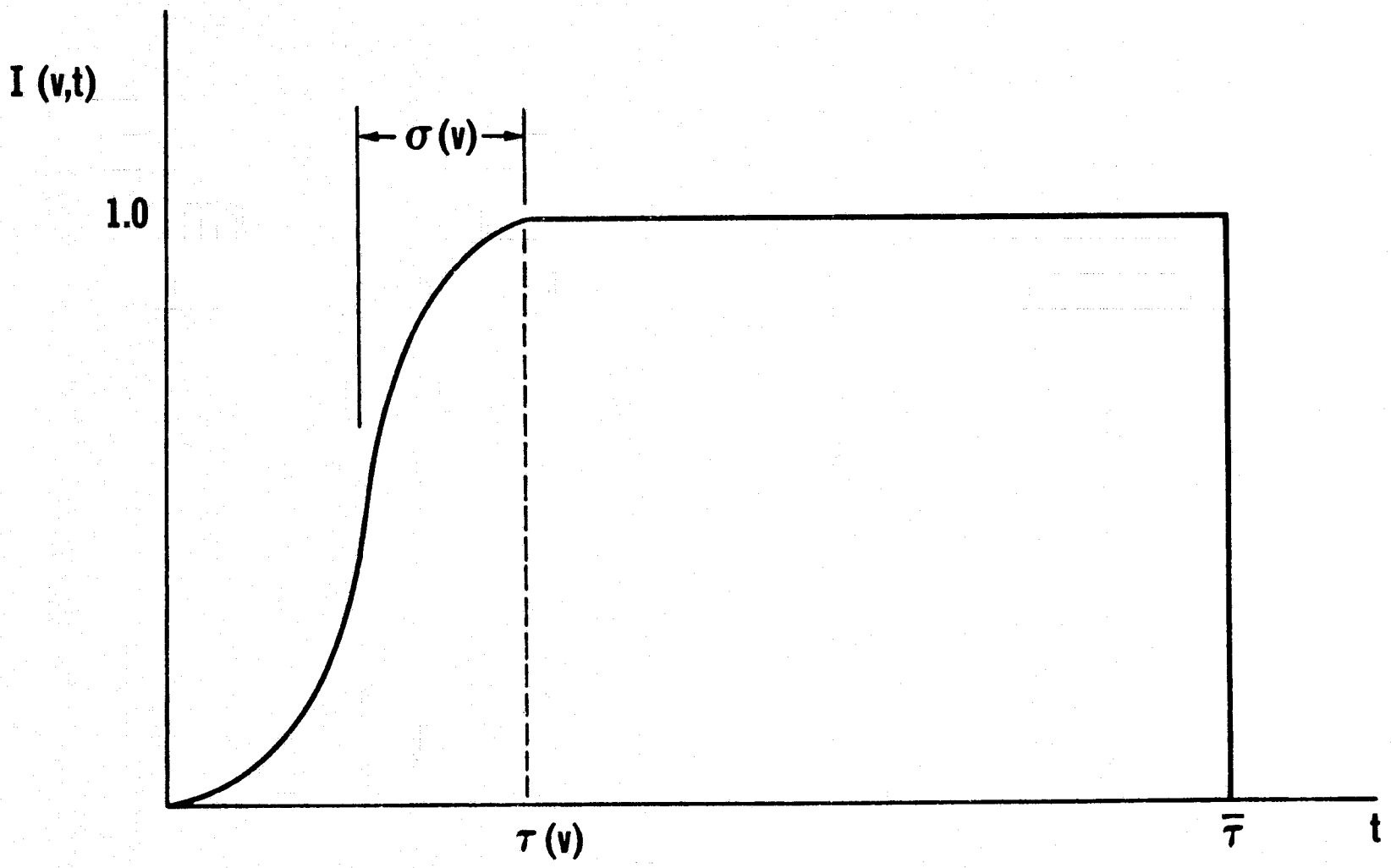

Figure 14